JHEP

Published for SISSA by Springer

Received: April 12, 2019
Accepted: April 26, 2019
Published: May 7, 2019

B_s mixing observables and $|V_{td}/V_{ts}|$ from sum rules

Daniel King,[a] **Alexander Lenz**[a] **and Thomas Rauh**[a,b]

[a] *IPPP, Department of Physics, University of Durham, Durhman DH1 3LE, U.K.*

[b] *Albert Einstein Center for Fundamental Physics, Institute for Theoretical Physics, University of Bern, Sidlerstrasse 5, CH-3012 Bern, Switzerland*

E-mail: daniel.j.king@durham.ac.uk, alexander.lenz@durham.ac.uk, rauh@itp.unibe.ch

Abstract: We consider the effects of a non-vanishing strange-quark mass in the determination of the full basis of dimension six matrix elements for B_s mixing, in particular we get for the ratio of the $V-A$ Bag parameter in the B_s and B_d system: $\overline{B}^s_{Q_1}/\overline{B}^d_{Q_1} = 0.987^{+0.007}_{-0.009}$. Combining these results with the most recent lattice values for the ratio of decay constants f_{B_s}/f_{B_d} we obtain the most precise determination of the ratio $\xi = f_{B_s}\sqrt{\overline{B}^s_{Q_1}}/f_{B_d}\sqrt{\overline{B}^d_{Q_1}} = 1.2014^{+0.0065}_{-0.0072}$ in agreement with recent lattice determinations. We find $\Delta M_s = (18.5^{+1.2}_{-1.5})\text{ps}^{-1}$ and $\Delta M_d = (0.547^{+0.035}_{-0.046})\text{ps}^{-1}$ to be consistent with experiments at below one sigma. Assuming the validity of the SM, our calculation can be used to directly determine the ratio of CKM elements $|V_{td}/V_{ts}| = 0.2045^{+0.0012}_{-0.0013}$, which is compatible with the results from the CKM fitting groups, but again more precise.

Keywords: Effective Field Theories, Heavy Quark Physics, Nonperturbative Effects, Perturbative QCD

ArXiv ePrint: 1904.00940

https://doi.org/10.1007/JHEP05(2019)034

JHEP05(2019)034

Contents

1 Introduction

Mixing of B_s mesons is experimentally well studied [1] and the mass difference $\Delta M_s = 2|M_{12}^s|$ is known with a high precision [2] (based on the individual measurements [3–7]):

$$\Delta M_s^{\text{Exp.}} = (17.757 \pm 0.021)\,\text{ps}^{-1}\,. \tag{1.1}$$

The corresponding theory expression for M_{12}^s reads

$$M_{12}^s = \frac{G_F^2}{12\pi^2}\lambda_t^2 M_W^2 S_0(x_t)\hat{\eta}_B B f_{B_s}^2 M_{B_s}\,, \tag{1.2}$$

with the CKM element $\lambda_t = V_{ts}^* V_{tb}$ and the Inami-Lim function S_0 [8] describing the result of the 1-loop box diagrams in the standard model (SM). Perturbative 2-loop QCD corrections are compressed in the factor $\hat{\eta}_B$ [9]. Since this observable is loop-suppressed in the SM, it is expected to be very sensitive to BSM effects. The bag parameter $B \equiv \overline{B}_{Q_1}^s$ and the decay constant f_{B_s} quantify the hadronic contribution to B-mixing; the uncertainties of their numerical values make up the biggest uncertainty by far in the SM prediction of the mass difference. These parameters have been determined by lattice simulations [10–12] and for the case of B_d mesons with HQET sum rules [13–16]. There is also a recent lattice determination of the SU(3) breaking ratios [17].

JHEP05(2019)034

Taking the most recent lattice average from the Flavour Lattice Averaging Group (FLAG) [18], which is more or less equivalent to the result in [12], one gets [19] a SM prediction for the mass difference, which is larger than the measurement:

$$\Delta M_s^{\mathrm{SM},2017} = (20.01 \pm 1.25)\,\mathrm{ps}^{-1}\,. \tag{1.3}$$

Such a value has dramatic consequences for some of the BSM models that are currently investigated in order to explain the flavour anomalies. In particular the parameter space of certain Z' models is almost completely excluded [19].

In this work we extend the analysis of [15] with effects of a finite strange-quark mass, thus getting for the first time a HQET sum rule prediction for the mixing Bag parameter of B_s mesons. Lattice simulations typically achieve a much higher precision than sum rule calculations, but in our case a sum rule for $B-1$ can be written down. Since the value of the Bag parameter B is close to 1, even a moderate precision of the sum rule of the order of 20 % for $B-1$, turns into a precision of the order of 2% for the whole Bag parameter, which is highly competitive. Thus our determination constitutes an independent cross-check of the large lattice value found in [12]. In combination with a precise lattice determination of the decay constant f_{B_s} our result for the Bag parameter can also be used for a direct determination of $|V_{ts}^* V_{tb}|$ from the measured mass difference $\Delta M_s^{\mathrm{Exp.}}$. Taking instead a ratio of the mass differences in the B_d and the B_s system one can get a clean handle on $|V_{td}/V_{ts}|$. Taking further a ratio of ΔM_s and the rare branching ratio $Br(B_s \to \mu^+\mu^-)$ the decay constant and the CKM dependence cancel and the Bag parameter will be the only relevant input parameter.

Our paper is organised as follows: in section 2 we set up the sum rule for the Bag parameter and determine the m_s corrections, in section 3 we present a numerical study of the sum rules and we perform a phenomenological analysis. Finally, we conclude in section 4.

2 Sum rules in HQET

2.1 Operator basis and definition of bag parameters

In this work we use the full dimension-six $\Delta B = 2$ operator basis required for a calculation of ΔM_s in the SM[1] and BSM theories and for a SM prediction of $\Delta\Gamma_s$. The QCD operators involved are

$$\begin{aligned}
Q_1 &= \bar{b}_i\gamma_\mu(1-\gamma^5)s_i\ \bar{b}_j\gamma^\mu(1-\gamma^5)s_j, \\
Q_2 &= \bar{b}_i(1-\gamma^5)s_i\ \bar{b}_j(1-\gamma^5)s_j, \qquad & Q_3 &= \bar{b}_i(1-\gamma^5)s_j\ \bar{b}_j(1-\gamma^5)s_i, \\
Q_4 &= \bar{b}_i(1-\gamma^5)s_i\ \bar{b}_j(1+\gamma^5)s_j, \qquad & Q_5 &= \bar{b}_i(1-\gamma^5)s_j\ \bar{b}_j(1+\gamma^5)s_i.
\end{aligned} \tag{2.1}$$

while our HQET basis is defined as

$$\begin{aligned}
\tilde{Q}_1 &= \bar{h}_i^{\{(+)}\gamma_\mu(1-\gamma^5)s_i\ \bar{h}_j^{(-)\}}\gamma^\mu(1-\gamma^5)s_j, \qquad & \tilde{Q}_2 &= \bar{h}_i^{\{(+)}(1-\gamma^5)s_i\ \bar{h}_j^{(-)\}}(1-\gamma^5)s_j, \\
\tilde{Q}_4 &= \bar{h}_i^{\{(+)}(1-\gamma^5)s_i\ \bar{h}_j^{(-)\}}(1+\gamma^5)s_j, \qquad & \tilde{Q}_5 &= \bar{h}_i^{\{(+)}(1-\gamma^5)s_j\ \bar{h}_j^{(-)\}}(1+\gamma^5)s_i,
\end{aligned} \tag{2.2}$$

[1] The operator Q_1 corresponds to the SM contribution to ΔM_s.

JHEP05(2019)034

where $h^{(+/-)}(x)$ is the HQET bottom/anti-bottom field and we use the notation

$$\bar{h}^{\{(+)}\Gamma_A s\ \bar{h}^{(-)\}}\Gamma_B s = \bar{h}^{(+)}\Gamma_A s\ \bar{h}^{(-)}\Gamma_B s + \bar{h}^{(-)}\Gamma_A s\ \bar{h}^{(+)}\Gamma_B s. \tag{2.3}$$

The matching condition is given by

$$\langle Q_i \rangle (\mu) = \sum C_{Q_i \tilde{Q}_j} \langle \tilde{Q}_j \rangle + \mathcal{O}(1/m_b), \tag{2.4}$$

for which the NLO HQET-QCD matching coefficients $C_{Q\tilde{Q}}$ were presented in [15]. We also use the same basis of evanescent operators. As mentioned in [15], the HQET evanescent operators are defined up to 3 constants a_i with $i = 1, 2, 3$ in order to gauge the scheme dependence. We also note that in all of the following we work within the NDR scheme in dimensional regularisation with $d = 4 - 2\epsilon$.

The QCD bag parameters B^s_Q are defined through [20]

$$\langle Q(\mu) \rangle = A_Q\, f_{B_s}^2 M_{B_s}^2\, B^s_Q(\mu) = \overline{A}_Q(\mu)\, f_{B_s}^2 M_{B_s}^2\, \overline{B}^s_Q(\mu), \tag{2.5}$$

with the coefficients A_Q given by

$$\begin{aligned}
A_{Q_1} &= 2 + \frac{2}{N_c}, \\
A_{Q_2} &= \frac{M_{B_s}^2}{(m_b + m_s)^2}\left(-2 + \frac{1}{N_c}\right), & A_{Q_3} &= \frac{M_{B_s}^2}{(m_b + m_s)^2}\left(1 - \frac{2}{N_c}\right), \\
A_{Q_4} &= \frac{2M_{B_s}^2}{(m_b + m_s)^2} + \frac{1}{N_c}, & A_{Q_5} &= 1 + \frac{2M_{B_s}^2}{N_c(m_b + m_s)^2},
\end{aligned} \tag{2.6}$$

where M_{B_s} denotes the B_s meson mass, m_q corresponds to quark pole masses and the B_s meson decay constant f_{B_s} is defined by

$$\langle 0|\bar{b}\gamma^\mu\gamma^5 s|B_s(p)\rangle = -i f_{B_s} p^\mu. \tag{2.7}$$

The barred terms in the far right expression of (2.5) indicate that the quark masses used there are in the $\overline{\text{MS}}$ scheme. For the reasons discussed in [15] we prefer to use the pole masses for our analysis and then convert to this form at the end. Similarly, the HQET bag parameters are defined through

$$\langle\!\langle \tilde{Q}(\mu) \rangle\!\rangle = A_{\tilde{Q}}\, F_s^2(\mu)\, B^s_{\tilde{Q}}(\mu), \tag{2.8}$$

with the coefficients $A_{\tilde{Q}}$ given by

$$A_{\tilde{Q}_1} = 2 + \frac{2}{N_c}, \quad A_{\tilde{Q}_2} = -2 + \frac{1}{N_c}, \quad A_{\tilde{Q}_4} = 2 + \frac{1}{N_c}, \quad A_{\tilde{Q}_5} = 1 + \frac{2}{N_c}, \tag{2.9}$$

and where the matrix elements are taken between non-relativistically normalised states $\langle\!\langle \tilde{Q}(\mu) \rangle\!\rangle \equiv \langle \overline{\mathbf{B}}_s | \tilde{Q}(\mu) | \mathbf{B}_s \rangle$ with

$$|B_s(p)\rangle = \sqrt{2M_{B_s}}|\mathbf{B}_s(v)\rangle + \mathcal{O}(1/m_b). \tag{2.10}$$

JHEP05(2019)034

The HQET decay constant $F_s(\mu)$, appearing in (2.8) is defined by

$$\langle 0|\bar{h}^{(-)}\gamma^\mu\gamma^5 s|\mathbf{B}_s(v)\rangle = -iF_s(\mu)v^\mu, \tag{2.11}$$

which is then related to the QCD decay constant f_{B_s} through

$$f_{B_s} = \sqrt{\frac{2}{M_{B_s}}}C(\mu)F_s(\mu) + \mathcal{O}\left(1/m_b\right), \tag{2.12}$$

with [21]

$$C(\mu) = 1 - 2C_F\frac{\alpha_s(\mu)}{4\pi} + \mathcal{O}(\alpha_s^2). \tag{2.13}$$

From our sum rule analysis we determine the HQET bag parameters $B^s_{\tilde{Q}}$. Using (2.4), (2.5), (2.8), and (2.12) we arrive at the relation

$$B^s_{\tilde{Q}_i}(\mu) = \sum_j \frac{A_{\tilde{Q}_j}}{A_{Q_i}}\frac{C_{Q_i\tilde{Q}_j}(\mu)}{C^2(\mu)}B^s_{\tilde{Q}_j}(\mu) + \mathcal{O}(1/m_b), \tag{2.14}$$

which allows us to then match the values of $B^s_{\tilde{Q}}$ onto their QCD counterparts.

2.2 Finite m_s effects in the HQET decay constant

To illustrate our strategy for the treatment of finite m_s effects we first consider the Borel sum rule for the HQET decay constant F_s which has been derived in [22–24]. In the B_s system it takes the form

$$F_s^2(\mu_\rho)e^{-\frac{\overline{\Lambda}+m_s}{t}} = \int_0^{\omega_c} d\omega\, e^{-\frac{\omega}{t}}\rho_\Pi(\omega)\,, \tag{2.15}$$

where ρ_Π is the discontinuity of the two-point correlator

$$\Pi(\omega) = i\int d^dx e^{ipx}\,\langle 0|\mathrm{T}\left[\tilde{j}_+^\dagger(0)\tilde{j}_+(x)\right]|0\rangle\,, \tag{2.16}$$

with $\omega = p\cdot v$ and the interpolating current $\tilde{j}_+ = \bar{s}\gamma^5 h^{(+)}$. The leading perturbative part of the discontinuity is given by

$$\rho_\Pi^{\mathrm{pert}}(\omega) = \frac{N_c}{2\pi^2}\left[(\omega+m_s)\sqrt{\omega^2-m_s^2}\,\theta(\omega-m_s) + \mathcal{O}(\alpha_s)\right]\,. \tag{2.17}$$

In the remainder of this subsection we consider the finite-energy (FESR) version of the sum rule (2.15) which is given by the limit $t\to\infty$ to be able to present compact analytic results. We obtain

$$\begin{aligned} F_s^2(\mu_\rho)|_{\mathrm{FESR}} &= \frac{N_c}{6\pi^2}\Bigg[\left(\omega_c - \frac{m_s}{2}\right)(\omega_c+2m_s)\sqrt{\omega_c^2-m_s^2} \\ &\qquad + \frac{3m_s^3}{2}\ln\left(\frac{m_s}{\omega_c+\sqrt{\omega_c^2-m_s^2}}\right) + \mathcal{O}(\alpha_s) + [\text{condensates}]\Bigg] \\ &= \frac{N_c\omega_c^3}{6\pi^2}\left[1+\frac{3m_s}{2\omega_c} - \frac{3m_s^2}{2\omega_c^2} - \frac{3m_s^3}{4\omega_c^3}\left(1-\ln\frac{m_s^2}{4\omega_c^2}\right) + \ldots\right]\,. \end{aligned} \tag{2.18}$$

JHEP05(2019)034

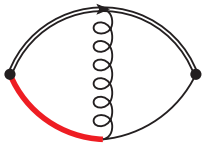

Figure 1. Sample diagram involving a soft light-quark propagator (red thick line).

In the last step we have expanded the result in the small ratio $m_s/\omega_c \sim 0.1$. The appearance of a $m_s^3 \ln(m_s)$ term in the expansion indicates that energies ω of the order m_s contribute at order m_s^3. These logarithms can be absorbed into the quark condensate [22, 25]. In the following we show how the terms up to order m_s^2 can be determined without knowing the full m_s dependence of the discontinuity (2.17). This will be essential for the determination of the m_s effects in the Bag parameters where the calculation of the full m_s dependence is very challenging (3 loops and 3 scales). We first split the integration at an arbitrary scale ν with $m_s \ll \nu \ll \omega_c$. Above ν we may expand the integrand in m_s/ω, yielding the identity

$$\mathcal{T}_{\frac{m_s}{\omega_c}}[F_s^2(\mu_\rho)]e^{-\frac{\bar{\Lambda}+m_s}{t}} = \mathcal{T}_{\{\frac{m_s}{\omega_c},\frac{m_s}{\nu},\frac{\nu}{\omega_c}\}}\left[\int_{m_s}^{\nu} d\omega\, e^{-\frac{\omega}{t}}\rho_\Pi(\omega) + \int_{\nu}^{\omega_c} d\omega\, e^{-\frac{\omega}{t}}\mathcal{T}_{\frac{m_s}{\omega}}[\rho_\Pi(\omega)]\right], \tag{2.19}$$

where $\mathcal{T}_x[\dots]$ indicates that the expression in square brackets must be Taylor expanded in x. The dependence on the scale ν has to cancel in the expanded result. We can therefore take the limit $\nu \to m_s$ *after* expanding the result according to the scaling $m_s \ll \nu \ll \omega_c$. We note that the contribution from the integration of the full integrand between m_s and ν does not vanish for $\nu \to m_s$, because the limit has to be taken after the expansion in m_s and the two operations do not commute. It is however clear from dimensional analysis that this contribution must be polynomial in m_s starting at m_s^3 since the exponential can be Taylor expanded. This demonstrates that it is sufficient to compute the discontinuity (2.17) as an expansion in m_s/ω if we restrict the analysis to the linear and quadratic terms which is clearly sufficient due to the small expansion parameter. In the FESR limit considered above we find[2]

$$\mathcal{T}_{\frac{m_s}{\omega_c}}\left[\int_{m_s}^{\omega_c} d\omega\, \mathcal{T}_{\frac{m_s}{\omega}}[\rho_\Pi(\omega)]\right] = \frac{N_c\omega_c^3}{6\pi^2}\left[1+\frac{3m_s}{2\omega_c}-\frac{3m_s^2}{2\omega_c^2}-\frac{m_s^3}{\omega_c^3}\left(1-\frac{3}{4}\ln\frac{m_s^2}{\omega_c^2}\right)+\dots\right]. \tag{2.20}$$

The difference between (2.18) and (2.20) is indeed of order m_s^3 and is compensated by the contribution from the first term on the right-hand side of (2.19).

At NLO we therefore only compute the expanded result by using the method of regions [26, 27]. The light degrees of freedom can be either hard with momentum $k \sim \omega$ or soft with momentum $k \sim m_s$ whereas the heavy quark field is always hard. Up to and including the order m_s^2 there are however only contributions from diagrams where all lines are hard. An example diagram involving a soft line is shown in figure 1. The integral measure scales as m_s^4 and the soft light-quark propagator scales as m_s^{-1}, yielding an overall scaling of m_s^3. Diagrams where only the gluon is soft are scaleless and vanish in dimen-

[2]Here the limit $\nu \to m_s$ and the Taylor expansion commute, because the integrand is polynomial in m_s.

JHEP05(2019)034

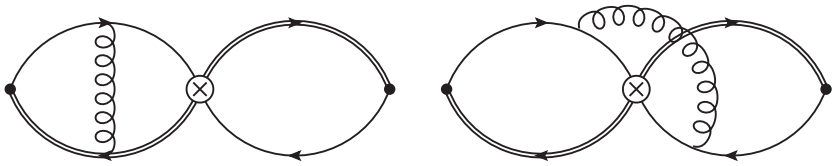

Figure 2. Examples for factorizing (left) and non-factorizing (right) contributions to the three-point correlator (2.22) at NLO in α_s.

sional regularization. Contributions where both loop momenta are soft are of the order m_s^4. Therefore, we only need to consider the fully hard momentum region where the integrand can be naively Taylor expanded in m_s. We obtain

$$\begin{aligned}\rho_\Pi(\omega) &\equiv \frac{\Pi(\omega+i0)-\Pi(\omega-i0)}{2\pi i} \\ &= \frac{N_c\omega^2}{2\pi^2}\,\theta(\omega-m_s)\bigg\{1+\frac{m_s}{\omega}-\frac{1}{2}\left(\frac{m_s}{\omega}\right)^2+\dots \\ &\quad+\frac{\alpha_s C_F}{4\pi}\left[17+\frac{4\pi^2}{3}+3\ln\frac{\mu_\rho^2}{4\omega^2}+\left(20+\frac{4\pi^2}{3}+6\ln\frac{\mu_\rho^2}{4\omega^2}-3\ln\frac{\mu_\rho^2}{m_s^2}\right)\frac{m_s}{\omega}\right. \\ &\quad\left.+\left(1-\frac{9}{2}\ln\frac{\mu_\rho^2}{4\omega^2}+3\ln\frac{\mu_\rho^2}{m_s^2}\right)\left(\frac{m_s}{\omega}\right)^2+\dots\right]+\mathcal{O}(\alpha_s^2)\bigg\}+[\text{condensates}],\end{aligned} \tag{2.21}$$

in agreement with [22].

2.3 Finite m_s effects in the Bag parameters

The sum rule for the Bag parameters is based on the three-point correlator

$$K_{\tilde{Q}}(\omega_1,\omega_2)=\int d^dx_1 d^dx_2 e^{ip_1\cdot x_1-ip_2\cdot x_2}\,\langle 0|\mathrm{T}\left[\tilde{j}_+(x_2)\tilde{Q}(0)\tilde{j}_-(x_1)\right]|0\rangle\,, \tag{2.22}$$

where $\omega_{1,2}=p_{1,2}\cdot v$ and the interpolating currents for the $\overline{B}_s$ and B_s mesons read

$$\tilde{j}_+=\bar{s}\gamma^5 h^{(+)},\qquad \tilde{j}_-=\bar{s}\gamma^5 h^{(-)}. \tag{2.23}$$

The accuracy of the sum rule approach crucially depends on the observation that the contributions to the correlator can be split into factorizable and non-factorizable ones, examples of which are given in figure 2.22. The full set of factorizable contributions amounts to $B^s_{\tilde{Q}}=1$ which allows us to formulate a sum rule for the deviation $\Delta B^s_{\tilde{Q}}=B^s_{\tilde{Q}}-1$ based only on the non-factorizable contributions [13, 15, 28, 29]

$$\Delta B^s_{\tilde{Q}_i}(\mu_\rho)=\frac{1}{A_{\tilde{Q}_i}F_s(\mu_\rho)^4}\int_0^{\omega_c}d\omega_1 d\omega_2 e^{\frac{\overline{\Lambda}+m_s-\omega_1}{t_1}+\frac{\overline{\Lambda}+m_s-\omega_2}{t_2}}\Delta\rho_{\tilde{Q}_i}(\omega_1,\omega_2) \tag{2.24}$$

$$=\frac{1}{A_{\tilde{Q}_i}}\frac{\int_0^{\omega_c}d\omega_1 d\omega_2 e^{-\frac{\omega_1}{t_1}-\frac{\omega_2}{t_2}}\Delta\rho_{\tilde{Q}_i}(\omega_1,\omega_2)}{\left(\int_0^{\omega_c}d\omega_1 e^{-\frac{\omega_1}{t_1}}\rho_\Pi(\omega_1)\right)\left(\int_0^{\omega_c}d\omega_2 e^{-\frac{\omega_2}{t_2}}\rho_\Pi(\omega_2)\right)}. \tag{2.25}$$

JHEP05(2019)034

where the second equation makes use of (2.15). The quantity $\Delta\rho_{\tilde{Q}_i}$ is the non-factorizable part of the double discontinuity

$$\rho_{\tilde{Q}_i}(\omega_1,\omega_2) = A_{\tilde{Q}_i}\rho_\Pi(\omega_1)\rho_\Pi(\omega_2) + \Delta\rho_{\tilde{Q}_i}\,. \tag{2.26}$$

In [15] we derived a simple analytical result for the HQET bag parameters by comparing (2.24) to the square of the sum rule for the decay constant (2.15) with an appropriately chosen weight function

$$w_{\tilde{Q}_i}(\omega_1,\omega_2) = \frac{\Delta\rho^{\rm pert}_{\tilde{Q}_i}(\omega_1,\omega_2)}{\rho^{\rm pert}_\Pi(\omega_1)\rho^{\rm pert}_\Pi(\omega_2)}\,. \tag{2.27}$$

The generalization of this approach to the m_s corrections is straightforward. Expanding the double discontinuity in m_s, we obtain

$$\begin{aligned}\Delta\rho^{\rm pert}_{\tilde{Q}_i}(\omega_1,\omega_2) \equiv \frac{N_c C_F}{4}\frac{\omega_1^2\omega_2^2}{\pi^4}\frac{\alpha_s}{4\pi}\Bigg[r^{(0)}_{\tilde{Q}_i}(x,L_\omega) + \left(\frac{m_s}{\omega_1}+\frac{m_s}{\omega_2}\right) r^{(1)}_{\tilde{Q}_i}(x,L_\omega) \\ + \left(\frac{m_s^2}{\omega_1^2}+\frac{m_s^2}{\omega_2^2}\right) r^{(2)}_{\tilde{Q}_i}(x,L_\omega) + \dots\Bigg]\theta(\omega_1-m_s)\theta(\omega_2-m_s),\end{aligned} \tag{2.28}$$

where $x = \omega_2/\omega_1$ and $L_\omega = \ln(\mu_\rho^2/(4\omega_1\omega_2))$. With this parametrization, the symmetry of the three-point correlator under exchange of ω_1 and ω_2 manifests as a symmetry under $x \leftrightarrow 1/x$ of the $r^{(j)}_{\tilde{Q}_i}$. The result for the deviation of the Bag parameters from the VSA reads

$$\begin{aligned}\Delta B^{s,\rm pert}_{\tilde{Q}_i}(\mu_\rho) &= \frac{w_{\tilde{Q}_i}(\overline{\Lambda}+m_s,\overline{\Lambda}+m_s)}{A_{\tilde{Q}_i}} \\ &= \frac{C_F}{N_c A_{\tilde{Q}_i}}\frac{\alpha_s(\mu_\rho)}{4\pi}\Bigg\{r^{(0)}_{\tilde{Q}_i}\left(1,L_{\overline{\Lambda}+m_s}\right) \\ &\quad + \frac{2m_s}{\overline{\Lambda}+m_s}\left[r^{(1)}_{\tilde{Q}_i}\left(1,L_{\overline{\Lambda}+m_s}\right) - r^{(0)}_{\tilde{Q}_i}\left(1,L_{\overline{\Lambda}+m_s}\right)\right] \\ &\quad + \frac{2m_s^2}{(\overline{\Lambda}+m_s)^2}\left[r^{(2)}_{\tilde{Q}_i}\left(1,L_{\overline{\Lambda}+m_s}\right) - 2r^{(1)}_{\tilde{Q}_i}\left(1,L_{\overline{\Lambda}+m_s}\right) + 2r^{(0)}_{\tilde{Q}_i}\left(1,L_{\overline{\Lambda}+m_s}\right)\right] \\ &\quad + \dots\Bigg\},\end{aligned} \tag{2.29}$$

where $L_{\overline{\Lambda}+m_s} = \ln(\mu_\rho^2/(4(\overline{\Lambda}+m_s)^2))$. We find that the result only depends on the value of the double discontinuity at $\omega_1 = \omega_2 = \overline{\Lambda}+m_s$. Thus, the knowledge of the m_s-expanded double discontinuity is sufficient to determine the m_s effects for the Bag parameters in B_s mixing. However, the use of this weight function approach relies on the expanded version of the sum rule (2.15) for the decay constant. As discussed in the previous subsection, this approach gives an incorrect result at the order m_s^3 and the result (2.29) is therefore limited to the quadratic order in m_s.

2.4 Non-zero m_s corrections to the non-factorizable part

We compute the m_s-expanded result for the leading non-factorizable part of the three-point correlators using the expansion by regions [26, 27]. As in the case of the two-point

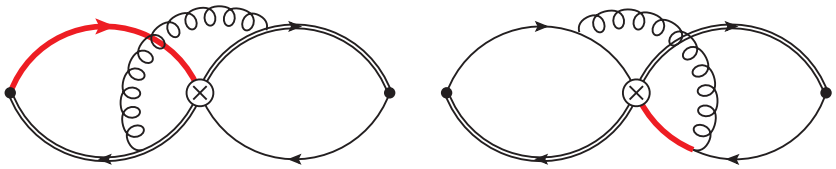

Figure 3. Examples for soft corrections to the non-factorizable part of the three-point correlator (2.22). The red, thick light-quark line carries momentum of the order of $m_s \ll \omega \sim \overline{\Lambda}$.

correlator, contributions involving soft propagators like the ones shown in figure 3 first contribute at order m_s^3. Thus, we only have to consider the fully hard momentum region where all loop momenta admit the scaling $l \sim \omega_i \gg m_s$ and the loop integrands can be naively Taylor expanded in m_s. We have performed two independent calculations. The amplitudes are either generated using `QGRAF` [30] with further processing in `Mathematica` or with a manual approach. The Dirac algebra is performed either with `TRACER` [31] or a private implementation. We employ `FIRE` [32] to generate IBP relations [33] between the loop integrals and to reduce them to a set of Master integrals with the Laporta algorithm [34]. The required master integrals have been computed to all orders in ϵ in [35]. We have expanded them up to the required order in ϵ using `HypExp` [36]. For completeness we state the results $r^{(0)}_{\tilde{Q}_i} = r^{(0)}_{\tilde{Q}_i}(x, L_\omega)$ for $m_s = 0$ previously presented in [15]

$$\begin{aligned}
r^{(0)}_{\tilde{Q}_1} &= 8 - \frac{a_2}{2} - \frac{8\pi^2}{3}, \\
r^{(0)}_{\tilde{Q}_2} &= 25 + \frac{a_1}{2} - \frac{4\pi^2}{3} + 6L_\omega + \phi(x), \\
r^{(0)}_{\tilde{Q}_4} &= 16 - \frac{a_3}{4} - \frac{4\pi^2}{3} + 3L_\omega + \frac{\phi(x)}{2}, \\
r^{(0)}_{\tilde{Q}_5} &= 29 - \frac{a_3}{2} - \frac{8\pi^2}{3} + 6L_\omega + \phi(x),
\end{aligned} \tag{2.30}$$

with

$$\phi(x) = \begin{cases} x^2 - 8x + 6\ln(x), & x \le 1, \\ \dfrac{1}{x^2} - \dfrac{8}{x} - 6\ln(x), & x > 1. \end{cases} \tag{2.31}$$

For the linear terms $r^{(1)}_{\tilde{Q}_i} = r^{(1)}_{\tilde{Q}_i}(x, L_\omega)$ we obtain

$$r^{(1)}_{\tilde{Q}_1} = -\frac{a_2}{2} - \frac{8\pi^2}{3} - 2\psi(x) + \begin{cases} \dfrac{2(18 - 63x + 23x^2)}{9(1+x)} + \left(2 - \dfrac{2(3+x^3)}{3x(1+x)}\right)\ln(x), & x \le 1, \\ \dfrac{2(23 - 63x + 18x^2)}{9x(1+x)} - \left(2 - \dfrac{2(1+3x^3)}{3x(1+x)}\right)\ln(x), & x > 1, \end{cases}$$

$$r^{(1)}_{\tilde{Q}_2} = \frac{a_1}{2} - \frac{4\pi^2}{3} + 6L_\omega + \psi(x) + \begin{cases} \dfrac{243 + 162x - 41x^2}{9(1+x)} + \left(5 + \dfrac{3+x^3}{3x(1+x)}\right)\ln(x), & x \le 1, \\ \dfrac{243x^2 + 162x - 41}{9x(1+x)} - \left(5 + \dfrac{1+3x^3}{3x(1+x)}\right)\ln(x), & x > 1, \end{cases}$$

JHEP05(2019)034

$$
\begin{aligned}
r^{(1)}_{\tilde{Q}_4} &= -\frac{a_3}{4} - \frac{4\pi^2}{3} + 3L_\omega + \begin{cases} \dfrac{4(36+9x+x^2)}{9(1+x)} + \left(3 - \dfrac{2x^2}{3(1+x)}\right)\ln(x), & x \le 1, \\ \dfrac{4(1+9x+36x^2)}{9x(1+x)} - \left(3 - \dfrac{2}{3x(1+x)}\right)\ln(x), & x > 1, \end{cases} \\
r^{(1)}_{\tilde{Q}_5} &= -\frac{a_3}{2} - \frac{8\pi^2}{3} + 6L_\omega + \begin{cases} \dfrac{29+11x-2x^2}{1+x} + 6\ln(x), & x \le 1, \\ \dfrac{29x^2+11x-2}{x(1+x)} - 6\ln(x), & x > 1, \end{cases}
\end{aligned} \tag{2.32}
$$

with

$$
\psi(x) = \begin{cases} \dfrac{(1-x)^2}{x}\left[2\ln(1-x) - \ln(x)\right], & x \le 1, \\ \dfrac{(1-x)^2}{x}\left[2\ln(x-1) - \ln(x)\right], & x > 1. \end{cases} \tag{2.33}
$$

Last but not least, our results for the quadratic terms $r^{(2)}_{\tilde{Q}_i} = r^{(2)}_{\tilde{Q}_i}(x, L_\omega)$ are

$$
\begin{aligned}
r^{(2)}_{\tilde{Q}_1} &= \frac{1}{1+x^2}\left[\frac{(1-x)^2 a_2}{4} + \frac{2\pi^2(1-4x+x^2)}{3} + 2x\psi(x)\left(2 + \frac{1+x}{1-x}\ln(x)\right)\right. \\
&\quad \left. + \begin{cases} -\frac{2(6+6x-x^2+2x^3)}{3} + 2(2-4x+x^2)\ln(x) - 4(1-x^2)\mathrm{Li}_2(1-1/x), & x \le 1, \\ -\frac{2(2-x+6x^2+6x^3)}{3x} - 2(1-4x+2x^2)\ln(x) + 4(1-x^2)\mathrm{Li}_2(1-x), & x > 1, \end{cases}\right], \\
r^{(2)}_{\tilde{Q}_2} &= \frac{1}{1+x^2}\left[\frac{-(1-x)^2 a_1}{4} - 3(1-x)^2 L_\omega + \frac{\pi^2(1-4x+x^2)}{3} + \frac{x(1+x)}{1-x}\ln(x)\psi(x)\right. \\
&\quad \left. + \begin{cases} -\frac{75-198x+89x^2-4x^3}{6} - (3-6x+2x^2)\ln(x) - 2(1-x^2)\mathrm{Li}_2(1-1/x), & x \le 1, \\ +\frac{4-89x+198x^2-75x^3}{6x} + (2-6x+3x^2)\ln(x) + 2(1-x^2)\mathrm{Li}_2(1-x), & x > 1, \end{cases}\right], \\
r^{(2)}_{\tilde{Q}_4} &= \frac{1}{1+x^2}\left[\frac{(1-x)^2 a_3}{8} - \frac{3(1-x)^2}{2}L_\omega + \frac{x\psi(x)}{2}\left(1 + \frac{3(1+x)}{1-x}\ln(x)\right)\right. \\
&\quad \left. + \begin{cases} -(1+8x-5x^2)\frac{\pi^2}{6} - \frac{24-48x+16x^2+x^3}{3} - (1+x^2)\ln(x) & \\ -(1-x^2)\ln^2(x) - 5(1-x^2)\mathrm{Li}_2(1-1/x), & x \le 1, \\ +(5-8x-x^2)\frac{\pi^2}{6} - \frac{1+16x-48x^2+24x^3}{3x} + (1+x^2)\ln(x) & \\ +(1-x^2)\ln^2(x) + 5(1-x^2)\mathrm{Li}_2(1-x), & x > 1, \end{cases}\right], \\
r^{(2)}_{\tilde{Q}_5} &= \frac{1}{1+x^2}\left[\frac{(1-x)^2 a_3}{4} - 3(1-x)^2 L_\omega + \frac{2\pi^2(1-4x+x^2)}{3}\right. \\
&\quad + 2x\psi(x)\left(1 + \frac{1+x}{1-x}\ln(x)\right) - \frac{29-62x+29x^2}{2} \\
&\quad \left. + \begin{cases} -(1-x)^2\ln(x) - 4(1-x^2)\mathrm{Li}_2(1-1/x), & x \le 1, \\ +(1-x)^2\ln(x) + 4(1-x^2)\mathrm{Li}_2(1-x), & x > 1, \end{cases}\right].
\end{aligned} \tag{2.34}
$$

JHEP05(2019)034

3 Results and phenomenology

We determine the Bag parameters in section 3.1, give our predictions for the B_s mixing observables in section 3.2 and use the results to determine the CKM elements $|V_{td}|$ and $|V_{ts}|$ in section 3.3 and the top-quark $\overline{\text{MS}}$ mass in section 3.4. We then present an alternative prediction of the branching ratios $\mathcal{B}(B_q \to \mu^+\mu^-)$ from the ratios $\mathcal{B}(B_q \to \mu^+\mu^-)/\Delta M_q$ in section 3.5. Our analysis strategy closely follows the one we used in [15] in the limit $m_s = 0$ and we only comment on where they differ due to the non-zero strange mass while referring to [15] for more details.

3.1 Bag parameters

We determine the HQET Bag parameters at the scale $\mu_\rho = 1.5\,\text{GeV}$ using the weight function approach (2.29). The strange-quark mass scheme in (2.29) is undetermined since any scheme change would only affect the expressions at higher orders which are not taken into account. We use the value in the $\overline{\text{MS}}$ scheme at the scale μ_ρ which is determined from the central value of the average $\overline{m}_s(2\,\text{GeV}) = (95^{+9}_{-3})\,\text{MeV}$ [37]. To account for the uncertainties related to the scheme choice and the truncation of the expansion in m_s we increase the parametric uncertainty and use $\overline{m}_s(2\,\text{GeV}) = (95 \pm 30)\,\text{MeV}$. To the perturbative part we add the condensate contributions [38, 39]. The lattice simulation [40] shows that light and strange quark condensates agree within uncertainties and their result for the strange-quark condensate has since been confirmed with a different method [41]. With the factorization hypothesis $\langle\bar{q}Gq\rangle = m_0^2\langle\bar{q}q\rangle$ the same holds for the quark-gluon condensate. We therefore assume the condensate corrections to be the same in the B^0 and B_s^0 systems. We obtain

$$
\begin{aligned}
B^s_{\tilde{Q}_1}(1.5\text{ GeV}) &= (0.910 - 0.016_{m_s} + 0.003_{m_s^2})^{+0.025}_{-0.036} \\
&= 0.897^{+0.002}_{-0.002}(\overline{\Lambda})^{+0.020}_{-0.020}(\text{intr.})^{+0.005}_{-0.005}(\text{cond.})^{+0.014}_{-0.029}(\mu_\rho)^{+0.003}_{-0.003}(m_s), \\
B^s_{\tilde{Q}_2}(1.5\text{ GeV}) &= (0.939 - 0.006_{m_s} + 0.002_{m_s^2})^{+0.027}_{-0.031} \\
&= 0.936^{+0.014}_{-0.016}(\overline{\Lambda})^{+0.020}_{-0.020}(\text{intr.})^{+0.004}_{-0.004}(\text{cond.})^{+0.011}_{-0.016}(\mu_\rho)^{+0.004}_{-0.004}(m_s), \\
B^s_{\tilde{Q}_4}(1.5\text{ GeV}) &= (1.003 - 0.004_{m_s} + 0.001_{m_s^2})^{+0.023}_{-0.023} \\
&= 1.000^{+0.005}_{-0.004}(\overline{\Lambda})^{+0.020}_{-0.020}(\text{intr.})^{+0.010}_{-0.010}(\text{cond.})^{+0.000}_{-0.002}(\mu_\rho)^{+0.003}_{-0.002}(m_s), \\
B^s_{\tilde{Q}_5}(1.5\text{ GeV}) &= (0.988 - 0.008_{m_s} + 0.000_{m_s^2})^{+0.028}_{-0.027} \\
&= 0.980^{+0.015}_{-0.012}(\overline{\Lambda})^{+0.020}_{-0.020}(\text{intr.})^{+0.010}_{-0.010}(\text{cond.})^{+0.000}_{-0.007}(\mu_\rho)^{+0.007}_{-0.006}(m_s),
\end{aligned}
\tag{3.1}
$$

where we have indicated the orders in m_s with subscripts and find good convergence of the expansion. The differences in the leading terms with respect to the results for B_d mixing obtained in [15] arise because the logarithms $L_{\overline{\Lambda}}$ are replaced by $L_{\overline{\Lambda}+m_s}$ which we do not expand in $m_s/\overline{\Lambda}$.

The results (3.1) are then evolved to the matching scale $\mu_m = \overline{m}_b(\overline{m}_b)$ where they are converted to QCD Bag parameters $B^s_{\tilde{Q}}$ using (2.14). We do not consider the effects of a non-zero strange-quark mass in the QCD-HQET matching. The matching corrections are

JHEP05(2019)034

of the order $\alpha_s(\overline{m}_b(\overline{m}_b))/\pi \times \overline{m}_s(\overline{m}_b)/\overline{m}_b(\overline{m}_b) \sim 0.001$ and therefore subleading compared to the linear terms $\alpha_s(\mu_\rho)/\pi \times \overline{m}_s(\mu_\rho)/(\overline{\Lambda} + \overline{m}_s(\mu_\rho)) \sim 0.019$ and even the quadratic terms $\alpha_s(\mu_\rho)/\pi \times [\overline{m}_s(\mu_\rho)/(\overline{\Lambda} + \overline{m}_s(\mu_\rho))]^2 \sim 0.003$ in the sum rule. We do not include this uncertainty as a separate contribution in our error analysis since it is covered by the conservative variation of the input value for m_s. Lastly, we convert the QCD Bag parameters to the usual convention which we denoted as $\overline{B}^s_Q$ in (2.5). We find

$$\begin{aligned}
\overline{B}^s_{Q_1}(\overline{m}_b(\overline{m}_b)) &= 0.858^{+0.051}_{-0.052} = (0.870 - 0.015_{m_s} + 0.002_{m_s^2})^{+0.022}_{-0.033}(\mathrm{SR})^{+0.046}_{-0.040}(\mathrm{M}),\\
\overline{B}^s_{Q_2}(\overline{m}_b(\overline{m}_b)) &= 0.854^{+0.079}_{-0.072} = (0.857 - 0.005_{m_s} + 0.002_{m_s^2})^{+0.026}_{-0.030}(\mathrm{SR})^{+0.074}_{-0.066}(\mathrm{M}),\\
\overline{B}^s_{Q_3}(\overline{m}_b(\overline{m}_b)) &= 0.907^{+0.164}_{-0.155} = (0.880 + 0.027_{m_s} + 0.000_{m_s^2})^{+0.124}_{-0.125}(\mathrm{SR})^{+0.107}_{-0.091}(\mathrm{M}),\\
\overline{B}^s_{Q_4}(\overline{m}_b(\overline{m}_b)) &= 1.039^{+0.092}_{-0.083} = (1.043 - 0.004_{m_s} + 0.001_{m_s^2})^{+0.024}_{-0.024}(\mathrm{SR})^{+0.088}_{-0.080}(\mathrm{M}),\\
\overline{B}^s_{Q_5}(\overline{m}_b(\overline{m}_b)) &= 1.050^{+0.081}_{-0.074} = (1.058 - 0.007_{m_s} + 0.000_{m_s^2})^{+0.025}_{-0.025}(\mathrm{SR})^{+0.077}_{-0.069}(\mathrm{M}),
\end{aligned} \tag{3.2}$$

where we have included the uncertainty from variation of $\overline{m}_s$ in the sum rule (SR) error and M denotes the uncertainty from the QCD-HQET matching. We compare our results to other determinations from lattice simulations [10–12] and sum rules [13] and the FLAG averages [18] in figure 4 and find very good agreement overall with similar uncertainties. We observe that the FNAL/MILC'16 value for $\overline{B}_{Q_1}$ is larger than all the other results — with respect to our value the difference corresponds to 1.1 sigma. We note that FNAL/MILC'16 determined the combination $f^2_{B_s}\overline{B}_{Q_1}$ and extracted the Bag parameter using the 2016 PDG average for the decay constant. They are currently working on a direct determination and, since their recent result [42] for f_{B_s} is larger than the PDG value used in [12], we expect the Bag parameter to go down. On the other hand our Bag parameters for $Q_{4,5}$ are in good agreement with FNAL/MILC'16, while there is a tension of more than two sigmas with respect to the results of ETM'14. Similar tensions have been observed in the Kaon system [43] where it was conjectured that a difference in intermediate renormalization schemes might be responsible. We also consider the ratios $\overline{B}^{s/d}_{Q_1} \equiv \overline{B}^s_{Q_1}/\overline{B}^d_{Q_1}$ of the Bag parameters in the B^0_s and B^0_d system where a large part of the uncertainties cancel

$$\begin{aligned}
\overline{B}^{s/d}_{Q_1}(\overline{m}_b(\overline{m}_b)) &= 0.987^{+0.007}_{-0.009} = (1.001 - 0.017_{m_s} + 0.003_{m_s^2})^{+0.007}_{-0.008}(\mathrm{SR})^{+0.002}_{-0.002}(\mathrm{M}),\\
\overline{B}^{s/d}_{Q_2}(\overline{m}_b(\overline{m}_b)) &= 1.013^{+0.010}_{-0.008} = (1.017 - 0.006_{m_s} + 0.002_{m_s^2})^{+0.009}_{-0.008}(\mathrm{SR})^{+0.002}_{-0.002}(\mathrm{M}),\\
\overline{B}^{s/d}_{Q_3}(\overline{m}_b(\overline{m}_b)) &= 1.108^{+0.068}_{-0.051} = (1.076 + 0.033_{m_s} - 0.001_{m_s^2})^{+0.068}_{-0.051}(\mathrm{SR})^{+0.007}_{-0.007}(\mathrm{M}),\\
\overline{B}^{s/d}_{Q_4}(\overline{m}_b(\overline{m}_b)) &= 0.991^{+0.007}_{-0.008} = (0.994 - 0.004_{m_s} + 0.001_{m_s^2})^{+0.006}_{-0.008}(\mathrm{SR})^{+0.002}_{-0.002}(\mathrm{M}),\\
\overline{B}^{s/d}_{Q_5}(\overline{m}_b(\overline{m}_b)) &= 0.979^{+0.010}_{-0.014} = (0.985 - 0.007_{m_s} + 0.000_{m_s^2})^{+0.010}_{-0.013}(\mathrm{SR})^{+0.002}_{-0.002}(\mathrm{M}).
\end{aligned} \tag{3.3}$$

The leading terms in the m_s-expansion differ from unity because we do not expand the logarithms $L_{\overline{\Lambda}+m_s}$ in $m_s/\overline{\Lambda}$. Compared to the absolute Bag parameters we reduce the intrinsic sum rule error to 0.005, the condensate error to 0.002 and the uncertainty due to power corrections to 0.002 since the respective uncertainties cancel to a large extend in

JHEP05(2019)034

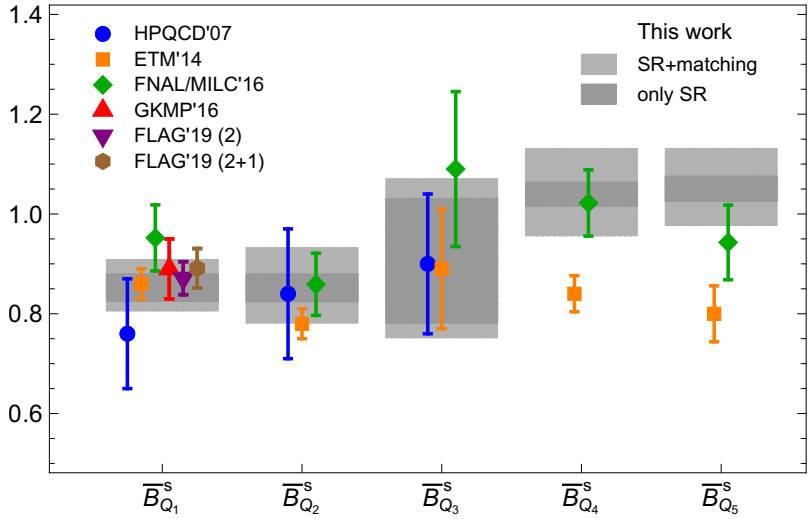

Figure 4. Comparison of Bag parameters relevant for B_s mixing. The dark gray regions indicate the ranges spanned only by the sum rule error whereas the light gray regions correspond to the total uncertainties. The sum rule value GKMP'16 corresponds to the result [13] for the B_d system with an uncertainty of ± 0.02 for the m_s effects added in quadrature as suggested by the authors in [14].

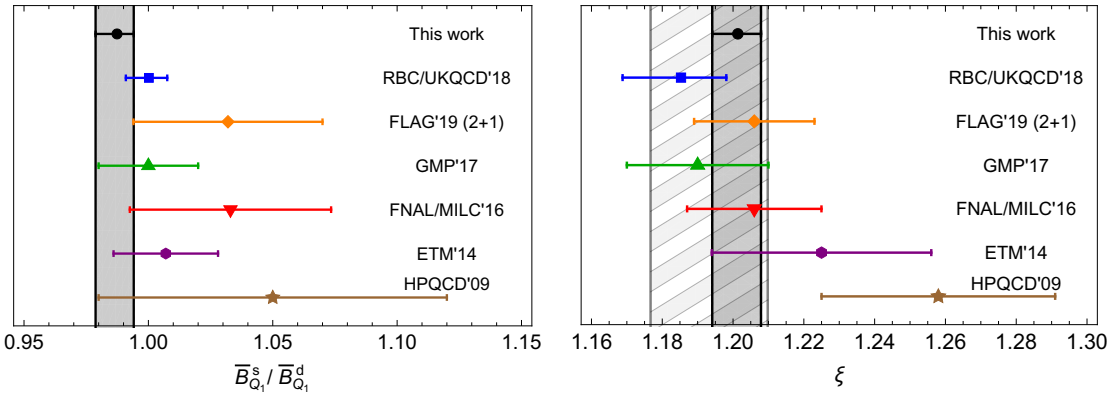

Figure 5. Comparison of the ratios $\overline{B}^s_{Q_1}/\overline{B}^d_{Q_1}$ and ξ defined in (3.4) with results from the literature [11, 12, 14, 17, 18, 45]. On the right side we also show our result obtained using the FLAG $N_f = 2+1$ average for the ratio of the decay constants as a hatched band. The GMP'17 [14] value for ξ corresponds to eq. (5.9) of that paper where the world average for f_{B_s}/f_B is used.

the ratios. However, we enhance the intrinsic sum rule and condensate error estimates for the operator Q_3 by a factor of five since the sum rule uncertainties for this operator are enhanced by large ratios of color factors $A_{Q_{1,2}}/A_{Q_3}$ as discussed in [15]. A detailed overview of the uncertainties is given in appendix A. The ratios (3.3) are in excellent agreement with the parametric estimates 1 ± 0.02 from [14, 15] with the exception of Q_3 where this uncertainty should have been enhanced like the other sum rule uncertainties listed above to account for the large color factors in the QCD-HQET matching relation (2.14) for the Bag parameter.

JHEP05(2019)034

Taking the FLAG [18][3] value with $N_f = 2+1+1$ for the ratio f_{B_s}/f_B of the decay constants of B_s^0 and B_d^0 we obtain the most precise result to date for the ratio

$$\xi \equiv \frac{f_{B_s}}{f_B}\sqrt{\overline{B}_{Q_1}^{s/d}} = 1.2014^{+0.0065}_{-0.0072} = 1.2014 \pm 0.0050 \left(\frac{f_{B_s}}{f_B}\right)^{+0.0043}_{-0.0053} \left(\overline{B}_{Q_1}^{s/d}\right), \tag{3.4}$$

where the ratio of decay constants and Bag parameters contributes equally to the error budget. A comparison with previous results is shown in figure 5. There we also show how the result changes when the FLAG $N_f = 2+1$ average is used for the ratio of the decay constants. Unfortunately FNAL/MILC and ETM do not provide values for $\overline{B}_{Q_i}^{s/d}$ for $i = 2,3,4,5$ so we cannot easily compare our results for these ratios.

3.2 B_s mixing observables

In this section we present the results of our B mixing analysis. We consider the mass differences ΔM_s and ΔM_d, the decay rate differences $\Delta\Gamma_s$ and $\Delta\Gamma_d$, and the ratio $\Delta M_s/\Delta M_d$, of which the latter benefits from a reduced uncertainty due to the cancellation of CKM factors and hadronic effects. For the bottom-quark mass we studied the $\overline{\text{MS}}$, PS [46], 1S [47] and the kinetic [48] mass schemes and found good agreement (see [15] for a more detailed discussion) - below we just quote the result in the PS scheme. We choose as our CKM parameter inputs the results of CKMfitter2018 [49] and collect these along with our other numerical inputs in appendix A. For the non-perturbative input we use our SR determination of the Bag parameters (eq. (3.2) and eq. (3.3)) together with the lattice decay constants ($N_f = 2+1+1$) from [18] (dominated by HPQCD'17 [44] and FNAL/MILC'17 [42]).

Comparing our findings for ΔM_s we see an excellent agreement with the experimental measurement [2]:

$$\begin{aligned}
\Delta M_s^{\text{exp}} &= (17.757 \pm 0.021)\,\text{ps}^{-1}, \\
\Delta M_s^{\text{SR}} &= (18.5^{+1.2}_{-1.5})\,\text{ps}^{-1} \\
&= (18.5 \pm 1.1\,(\text{had.}) \pm 0.1\,(\text{scale})^{+0.3}_{-1.0}\,(\text{param.}))\,\text{ps}^{-1}\,.
\end{aligned} \tag{3.5}$$

We note that the update to our CKM input gives rise to an increase in ΔM_s^{SR} from the value presented in [15], despite the inclusion of m_s-corrections which reduce the size of our hadronic input. Using instead the non-perturbative input purely from lattice determinations (FLAG 2019 [18], which is almost identical to the result in [12]), we get a considerably higher SM prediction for ΔM_s: $\Delta M_s^{\text{Lat.}} = (20.3^{+1.3}_{-1.7})\,\text{ps}^{-1} = (20.3 \pm 1.3\,(\text{had.}) \pm 0.1\,(\text{scale})^{+0.3}_{-1.1}\,(\text{param.}))\,\text{ps}^{-1}$, being about 1.5 standard deviations above the experiment. Due to updated CKM inputs this number is slightly larger than the one quoted in eq. (1.3). Averaging the SR and the lattice results, we get a further reduction of the uncertainties: $\Delta M_s^{\text{Av.}} = (19.4^{+1.0}_{-1.4})\,\text{ps}^{-1} = (19.4 \pm 0.9\,(\text{had.}) \pm 0.1\,(\text{scale})^{+0.3}_{-1.0}\,(\text{param.}))\,\text{ps}^{-1}$.

We also find perfect agreement between our result for $\Delta\Gamma_s$ and experiment [2]:

$$\begin{aligned}
\Delta\Gamma_s^{\text{exp}} &= (0.088 \pm 0.006)\,\text{ps}^{-1}, \\
\Delta\Gamma_s^{\text{SR}} &= (0.091^{+0.022}_{-0.030})\,\text{ps}^{-1} \\
&= (0.091 \pm 0.020\,(\text{had.})^{+0.008}_{-0.021}\,(\text{scale})^{+0.002}_{-0.005}\,(\text{param.}))\,\text{ps}^{-1}.
\end{aligned} \tag{3.6}$$

[3] The average is dominated by the HPQCD'17 [44] and FNAL/MILC'17 [42] results.

JHEP05(2019)034

Recent measurements [50, 51] that are not yet contained in the average [2] yield significantly smaller values for $\Delta\Gamma_s$ which are however still in the one-sigma range of our prediction. The theoretical prediction for the decay rate difference includes NLO QCD [52–55] and $1/m_b$ [56, 57] corrections. The latter depend on matrix elements of dimension-seven operators which are currently only known in the vacuum saturation approximation, which results in uncertainties of approximately 25-30%. The sizable scale uncertainty can be reduced with a NNLO computation of the HQE matching coefficients - first steps towards this have recently been performed in [58]. Using instead the non-perturbative input from lattice [18], we again get higher values $\Delta\Gamma_s^{\text{Lat.}} = (0.102^{+0.023}_{-0.032})\,\text{ps}^{-1} = (0.102 \pm 0.020\,(\text{had.})^{+0.010}_{-0.024}\,(\text{scale})^{+0.002}_{-0.006}\,(\text{param.}))\text{ps}^{-1}$. Due to the larger uncertainties this prediction overlaps at 1 sigma with experiment. Combining the the sum rule result with the lattice result we get $\Delta\Gamma_s^{\text{Av.}} = (0.097^{+0.022}_{-0.031})\,\text{ps}^{-1} = (0.097 \pm 0.020\,(\text{had.})^{+0.009}_{-0.023}\,(\text{scale})^{+0.002}_{-0.005}\,(\text{param.}))\,\text{ps}^{-1}$. Here the accuracy of the average does not improve, because the uncertainty is dominated by the unknown matrix elements of dimension seven operators and scale variation.

Due to new CKM inputs (compared to the B_d analysis in [15]), we are also updating our results for B_d mixing observables:[4]

$$\begin{aligned}\Delta M_d^{\text{exp}} &= (0.5064 \pm 0.0019)\,\text{ps}^{-1},\\ \Delta M_d^{\text{SR}} &= (0.547^{+0.035}_{-0.046})\,\text{ps}^{-1}\\ &= (0.547^{+0.033}_{-0.032}\,(\text{had.})^{+0.004}_{-0.002}\,(\text{scale})^{+0.011}_{-0.032}\,(\text{param.}))\,\text{ps}^{-1},\end{aligned} \tag{3.7}$$

and:[5]

$$\begin{aligned}\Delta\Gamma_d^{\text{exp}} &= (-1.3 \pm 6.6)\cdot 10^{-3}\,\text{ps}^{-1},\\ \Delta\Gamma_d^{\text{SR}} &= (2.6^{+0.6}_{-0.9})\cdot 10^{-3}\,\text{ps}^{-1}\\ &= (2.6 \pm 0.6\,(\text{had.})^{+0.2}_{-0.6}\,(\text{scale})^{+0.1}_{-0.2}\,(\text{param.}))\cdot 10^{-3}\,\text{ps}^{-1},\end{aligned} \tag{3.8}$$

where at present only an experimental upper bound on $\Delta\Gamma_d^{\text{exp}}$ is available. The SM value of the mass difference agrees with experiment at the 1 sigma level. Figure 6 (left panel) shows the comparison of the measurements of $\Delta\Gamma_s$ and ΔM_s with the corresponding theory predictions: in blue the 1 sigma region of our sum rule values, in the red the purely lattice results and in black the average of both. The right panel shows the same comparison for the B_d system. All in all the sum rule values agree well with experiment, while the pure lattice results show a 1.5 sigma deviation for the mass differences - leading to very strong bounds on BSM models that try to explain the flavour anomalies.

Finally, for the ratio of the mass differences we also find our results to be consistent (within about 1.3 standard deviations) with the measured value:

$$\begin{aligned}\left(\frac{\Delta M_d}{\Delta M_s}\right)_{\text{exp}} &= 0.0285 \pm 0.0001,\\ \left(\frac{\Delta M_d}{\Delta M_s}\right)_{\text{SR}} &= 0.0297^{+0.0006}_{-0.0009} = 0.0297^{+0.0004}_{-0.0003}\,(\text{had.})^{+0.0005}_{-0.0008}\,(\text{exp.}).\end{aligned} \tag{3.9}$$

[4] The corresponding lattice result reads $\Delta M_d^{\text{Lat.}} = (0.596^{+0.054}_{-0.063})\,\text{ps}^{-1}$ (about 1.4 sigma above experiment) and the average over SR and lattice is $\Delta M_d^{\text{Av.}} = (0.565^{+0.034}_{-0.046})\,\text{ps}^{-1}$.

[5] The corresponding lattice result reads $\Delta\Gamma_d^{\text{Lat.}} = (3.0^{+0.7}_{-1.0})\cdot 10^{-3}\,\text{ps}^{-1}$ and the average over SR and lattice is $\Delta\Gamma_d^{\text{Av.}} = (2.7^{+0.6}_{-0.9})\cdot 10^{-3}\,\text{ps}^{-1}$.

JHEP05(2019)034

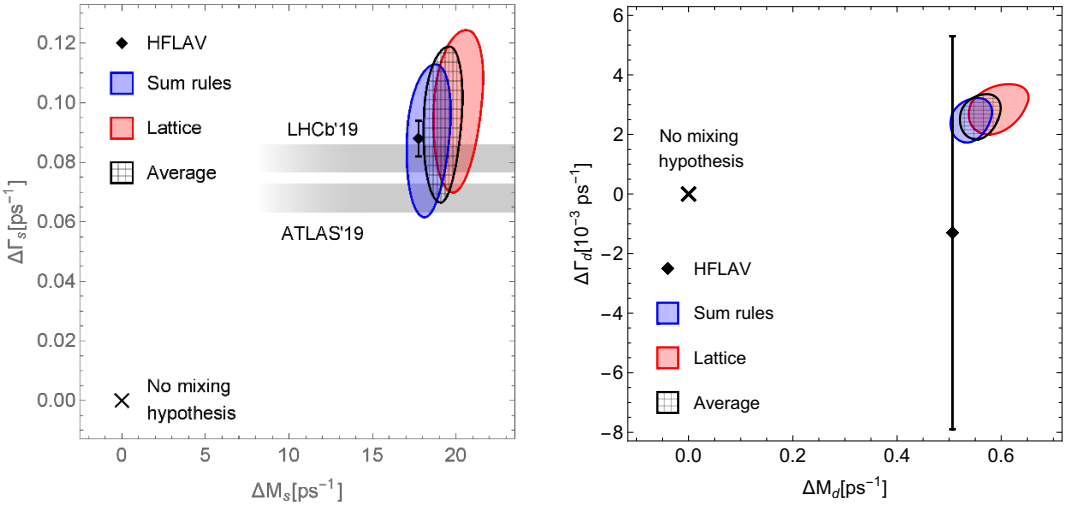

Figure 6. Our predictions (blue) for the mass and decay rate difference in the B_s (left) and B_d (right) systems are compared to the current experimental averages and the predictions (red) based on the latest lattice averages from FLAG [18] for $f_{B_q}^2 \overline{B}_{Q_1}^q$ and the FNAL/MILC'16 [12] results for $f_{B_q}^2 \overline{B}_{Q_i}^q$ with $i \neq 1$ and $\langle R_0 \rangle$. The weighted average over the sum rule and lattice results is shown in black. We indicate the updated Run 1 and Run 2 combinations for $\Delta\Gamma_s$ presented by LHCb [50] and ATLAS [51] at Moriond EW 2019 by shaded gray regions.

Due to our new value for ξ we get a theoretical precision of about 3% for the ratio of mass differences in the B_d and B_s systems, which poses severe constraints on BSM models, that modify neutral B meson mixing. The uncertainty is now dominated by the CKM factors. Using lattice inputs one gets a slightly less precise value $(\Delta M_d/\Delta M_s)_{\text{Lat.}} = 0.0295^{+0.0010}_{-0.0012} = 0.0295^{+0.0008}_{-0.0008}\,(\text{had.})^{+0.0005}_{-0.0008}\,(\text{exp.})$, which can be combined with the sum rule result to obtain $(\Delta M_d/\Delta M_s)_{\text{Av.}} = 0.0297^{+0.0006}_{-0.0009} = 0.0297^{+0.0003}_{-0.0003}\,(\text{had.})^{+0.0005}_{-0.0008}\,(\text{exp.})$.

3.3 Determination of the CKM elements $|V_{td}|$ and $|V_{ts}|$

We also can use the measured values of the mass differences, together with our bag parameter, the lattice results for the decay constant ($N_f = 2+1+1$ from [18, 42, 44]) and the value of the CKM element V_{tb} (from [49]) to determine $|V_{td}|$ and $|V_{ts}|$

$$\begin{aligned}
|V_{ts}|_{\text{SR}} &= (40.74^{+1.30}_{-1.21}) \cdot 10^{-3} \\
&= (40.74^{+1.29}_{-1.20}\,(\text{had.})\,^{+0.09}_{-0.14}\,(\mu)\,\pm 0.05\,(\text{param.})) \cdot 10^{-3}\,, \\
|V_{td}|_{\text{SR}} &= (8.36^{+0.26}_{-0.24}) \cdot 10^{-3} \\
&= (8.36^{+0.26}_{-0.24}\,(\text{had.})\,^{+0.02}_{-0.03}\,(\mu)\,\pm 0.02\,(\text{param.})) \cdot 10^{-3}\,.
\end{aligned} \tag{3.10}$$

These direct determinations overlap with the determinations based on CKM unitarity [49] (see [59] for similar results) but they are a little less precise:

$$\begin{aligned}
|V_{ts}|_{\text{CKMfitter}} &= (41.69^{+0.28}_{-1.08}) \cdot 10^{-3} \\
|V_{td}|_{\text{CKMfitter}} &= (8.710^{+0.086}_{-0.246}) \cdot 10^{-3}\,.
\end{aligned} \tag{3.11}$$

JHEP05(2019)034

We note that the results of the full CKM fit include data on B mixing and are therefore not completely independent. Thus, it is also interesting to compare to the results of the fit where only tree-level processes are considered. A discrepancy here would be a hint towards new physics in loop processes. The CKMfitter results are

$$\begin{aligned} |V_{ts}|_{\text{CKMfitter, tree}} &= (41.63^{+0.39}_{-1.45}) \cdot 10^{-3} \\ |V_{td}|_{\text{CKMfitter, tree}} &= (9.08^{+0.23}_{-0.45}) \cdot 10^{-3} \,. \end{aligned} \tag{3.12}$$

While there is good agreement for $|V_{ts}|$ the value of $|V_{td}|$ differs from our result by about 1.4 sigma. The value of the ratio $|V_{td}/V_{ts}|$ can be determined more precisely based on the exact relation

$$\frac{\Delta M_d}{\Delta M_s} = \left|\frac{V_{td}}{V_{ts}}\right|^2 \frac{1}{\xi^2} \frac{M_{B_d}}{M_{B_s}} \,. \tag{3.13}$$

Using our value of ξ from eq. (3.4) we can present here the most precise determination of $|V_{td}/V_{ts}|$:

$$|V_{td}/V_{ts}|_{\text{SR}} = 0.2045^{+0.0012}_{-0.0013} = 0.2045^{+0.0011}_{-0.0012}\,(\text{had.}) \pm 0.0004\,(\text{exp.})\,, \tag{3.14}$$

which is compatible with the values obtained by the FNAL/MILC [12] and RBC-UKQCD [17] collaborations

$$\begin{aligned} |V_{td}/V_{ts}| &= 0.2052 \pm 0.0033 && [\text{FNAL/MILC'16}]\,, \\ |V_{td}/V_{ts}| &= 0.2018^{+0.0020}_{-0.0027} && [\text{RBC-UKQCD'18}]\,. \end{aligned} \tag{3.15}$$

These values are all somewhat smaller than the expectation from CKM unitarity taken from CKMfitter [49] and UTfit [59]

$$\begin{aligned} |V_{td}/V_{ts}| &= 0.2088^{+0.0016}_{-0.0030} && [\text{CKMfitter}]\,, \\ |V_{td}/V_{ts}| &= 0.211 \pm 0.003 && [\text{UTfit}]\,. \end{aligned} \tag{3.16}$$

Compared to the CKMfitter result

$$|V_{td}/V_{ts}| = 0.2186^{+0.0049}_{-0.0059} \qquad [\text{CKMfitter, tree}]\,, \tag{3.17}$$

from the fit to tree-level processes our value (3.14) is smaller by about 2.3 standard deviations. Thus, an improved determination of $|V_{td}|$ and $|V_{td}/V_{ts}|$ from tree-level processes might provide an interesting hint towards new physics in the B_d system. Similar considerations have recently led to claims about an emerging ΔM_d anomaly [60].

An overview of the various results is presented in figure 7, where the overlap of the one-sigma regions for $|V_{td}|$, $|V_{ts}|$ and $|V_{td}/V_{ts}|$ is indicated by the shaded regions. Our results provide an important input for future CKM unitarity fits and can be used to extract the angle γ in the unitarity triangle from the linear dependency between ξ and the CKM angle γ observed in [61].

JHEP05(2019)034

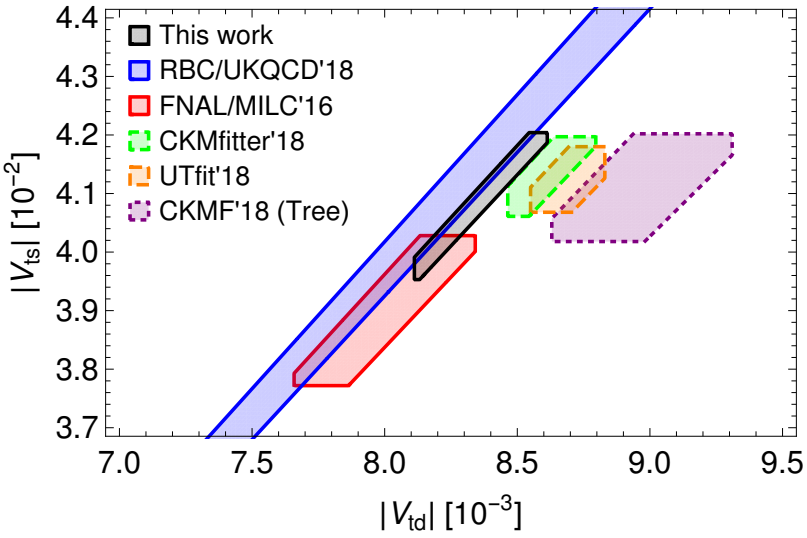

Figure 7. Comparison of our constraints on the CKM parameters $|V_{td}|$ and $|V_{ts}|$ with other works based on B mixing [12, 17] (solid boundaries) and unitarity [49, 59] (dashed boundaries). Since the full CKM fit includes the mass differences we also show the tree-level fit from CKMfitter [49] (dotted boundaries).

3.4 Determination of the top-quark $\overline{\text{MS}}$ mass

The parametric error from the top-quark mass currently dominates the uncertainty in the determination of the stability or meta-stability of the electroweak vacuum [62]. Direct measurements quote very precise values $m_t^{\text{MC}} = (173.0 \pm 0.4)\,\text{GeV}$ for the top quark mass [37], but these results correspond to so-called Monte-Carlo (MC) masses and not the top-quark pole mass. One therefore needs to account for additional uncertainties from the scheme conversion [63] when these values are used for phenomenological predictions. Alternatively one can determine the top-quark mass by fitting observables like the total top-pair production cross section which can be predicted in terms of the top-quark mass in a well-defined scheme like $\overline{\text{MS}}$. Similarly, we can use the mass differences ΔM_q for a theoretically clean determination of $\overline{m}_t(\overline{m}_t)$. Using the CKMfitter values for V_{td} and V_{ts} as input we obtain

$$\begin{aligned}
\overline{m}_t(\overline{m}_t) &= (158^{+9}_{-6})\,\text{GeV} = (158^{+7}_{-6}\,(\text{had.})^{+0}_{-1}\,(\mu)^{+6}_{-1}\,(\text{param.}))\,\text{GeV}, && \text{from } \Delta M_s, \\
\overline{m}_t(\overline{m}_t) &= (155^{+9}_{-6})\,\text{GeV} = (155^{+6}_{-6}\,(\text{had.})^{+0}_{-1}\,(\mu)^{+6}_{-2}\,(\text{param.}))\,\text{GeV}, && \text{from } \Delta M_d.
\end{aligned} \tag{3.18}$$

Combining both results we find

$$\overline{m}_t(\overline{m}_t) = (157^{+8}_{-6})\,\text{GeV} = (157^{+7}_{-6}\,(\text{had.})^{+0}_{-1}\,(\mu)^{+4}_{-1}\,(\text{param.}))\,\text{GeV}, \tag{3.19}$$

where we have averaged over the hadronic and scale uncertainties, which are correlated, and treated the parametric uncertainties, which are dominated either by V_{td} or V_{ts}, as independent. This is in good agreement with the PDG average [37]

$$\overline{m}_t(\overline{m}_t) = (160^{+5}_{-4})\,\text{GeV}, \tag{3.20}$$

JHEP05(2019)034

of $\overline{\text{MS}}$ mass determinations from cross section measurements with our uncertainty being about 50% larger. A very precise measurement of the top-quark PS or $\overline{\text{MS}}$ mass with a total uncertainty of about 50 MeV is possible at a future lepton collider running at the top threshold [64–66].

3.5 $\mathcal{B}(B_q \to \mu^+\mu^-)$

The branching ratio $\text{Br}(B_q \to l^+l^-)$ is strongly suppressed in the SM and theoretically clean. Thus, it provides a very sensitive probe for new physics. At present it has been computed at NNLO QCD plus NLO EW [67] and the dominant uncertainties are parametric, stemming from the decay constant and the CKM parameters. Both uncertainties cancel out of the ratio [68]

$$\frac{\text{Br}(B_q \to l^+l^-)}{\Delta M_q} = \frac{3G_F^2 M_W^2 m_l^2 \tau_{B_q^H}}{\pi^3} \sqrt{1 - \frac{4m_l^2}{M_{B_q}^2}} \frac{|C_A(\mu)|^2}{S_0(x_t)\hat{\eta}_B \overline{B}_{Q_1}^q(\mu)}\,, \tag{3.21}$$

which in turn receives its dominant uncertainty from the Bag parameter $\overline{B}_{Q_1}^q$. Using our result (3.3) and including the power-enhanced QED corrections determined in [69] we predict the branching ratio by multiplying (3.21) with the measured mass differences

$$\begin{aligned}
\text{Br}(B_s^0 \to \mu^+\mu^-)_{\text{SM}} &= (3.55^{+0.23}_{-0.20}) \cdot 10^{-9}\,, \\
\text{Br}(B_d^0 \to \mu^+\mu^-)_{\text{SM}} &= (9.40^{+0.58}_{-0.53}) \cdot 10^{-11}\,, \\
\left(\frac{\text{Br}(B_d^0 \to \mu^+\mu^-)}{\text{Br}(B_s^0 \to \mu^+\mu^-)}\right)_{\text{SM}} &= 0.0265 \pm 0.0003 = 0.0265 \pm 0.0002 \left(\overline{B}_{Q_1}^{s/d}\right) \pm 0.0002(\text{exp})\,,
\end{aligned} \tag{3.22}$$

where the uncertainties for the branching ratios are completely dominated by the error from $\overline{B}_{Q_1}^q$. The result for $B_s^0 \to \mu^+\mu^-$ is in good agreement with the current experimental average [2]

$$\text{Br}(B_s^0 \to \mu^+\mu^-)_{\text{exp}} = (3.1 \pm 0.7) \cdot 10^{-9}\,, \tag{3.23}$$

while the latest measurements only provide upper bounds at 95% confidence level for $B_d^0 \to \mu^+\mu^-$

$$\text{Br}(B_d^0 \to \mu^+\mu^-)_{\text{exp}} < \begin{cases} 11 \cdot 10^{-10}\,, & (\text{CMS [70]})\,, \\ 3.4 \cdot 10^{-10}\,, & (\text{LHCb [71]})\,, \\ 2.1 \cdot 10^{-10}\,, & (\text{ATLAS [72]})\,. \end{cases} \tag{3.24}$$

We compare our prediction (3.22) to the direct predictions from [42, 67, 69] which depend on the decay constants and CKM elements $|V_{tq}|$, the prediction [12] from the ratios $\text{Br}(B_q \to l^+l^-)/\Delta M_q$ and the experimental average (3.23) in figure 8. The shaded regions correspond to the overlap of the one-sigma regions for $\text{Br}(B_s^0 \to \mu^+\mu^-)$, $\text{Br}(B_d^0 \to \mu^+\mu^-)$ and $\text{Br}(B_d^0 \to \mu^+\mu^-)/\text{Br}(B_s^0 \to \mu^+\mu^-)$ where they were provided. We find good consistency among the various predictions with similar uncertainties for both approaches and good agreement with

JHEP05(2019)034

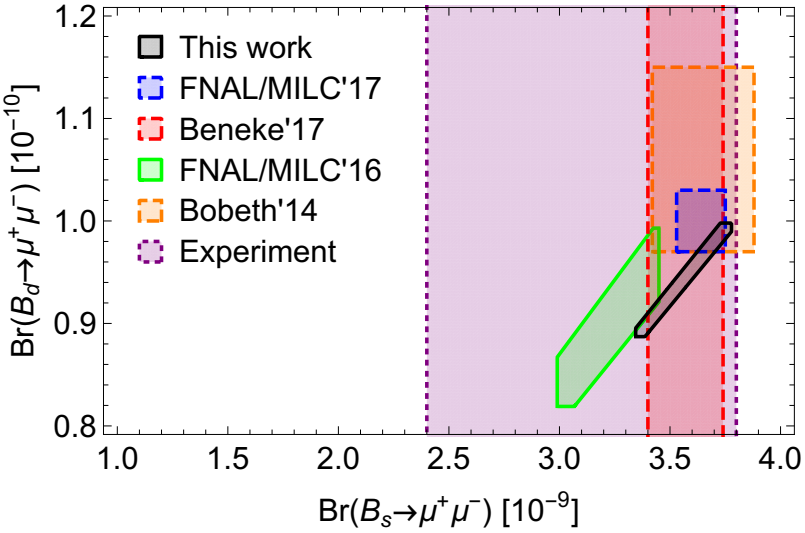

Figure 8. We compare our prediction for the branching ratios $\mathrm{Br}(B_q^0 \to \mu^+\mu^-)$ with $q = s, d$ to other predictions using either the decay constants [42, 67, 69] (dashed boundaries) or the Bag parameter $\overline{B}^q_{Q_1}$ [12] (solid boundaries) as input. The experimental average for $\mathrm{Br}(B_s^0 \to \mu^+\mu^-)$ is indicated by the region with the dotted boundary.

experiment whose uncertainty currently exceeds the theoretical one by a factor of about 3-4 in $\mathrm{Br}(B_s^0 \to \mu^+\mu^-)$.

For completeness we provide our predictions for the branching ratios to electrons

$$\begin{aligned}
\mathrm{Br}(B_s^0 \to e^+e^-)_{\mathrm{SM}} &= (8.37^{+0.55}_{-0.48}) \cdot 10^{-14}\,, \\
\mathrm{Br}(B_d^0 \to e^+e^-)_{\mathrm{SM}} &= (2.22^{+0.14}_{-0.13}) \cdot 10^{-15}\,, \\
\left(\frac{\mathrm{Br}(B_d^0 \to e^+e^-)}{\mathrm{Br}(B_s^0 \to e^+e^-)}\right)_{\mathrm{SM}} &= 0.0265 \pm 0.0003 = 0.0265 \pm 0.0002 \left(\overline{B}^{s/d}_{Q_1}\right) \pm 0.0002(\mathrm{exp})\,,
\end{aligned} \tag{3.25}$$

and tau leptons

$$\begin{aligned}
\mathrm{Br}(B_s^0 \to \tau^+\tau^-)_{\mathrm{SM}} &= (7.58^{+0.50}_{-0.44}) \cdot 10^{-7}\,, \\
\mathrm{Br}(B_d^0 \to \tau^+\tau^-)_{\mathrm{SM}} &= (1.98^{+0.12}_{-0.11}) \cdot 10^{-8}\,, \\
\left(\frac{\mathrm{Br}(B_d^0 \to \tau^+\tau^-)}{\mathrm{Br}(B_s^0 \to \tau^+\tau^-)}\right)_{\mathrm{SM}} &= 0.0262 \pm 0.0003 = 0.0262 \pm 0.0002 \left(\overline{B}^{s/d}_{Q_1}\right) \pm 0.0002(\mathrm{exp})\,.
\end{aligned} \tag{3.26}$$

4 Conclusions

We have presented in this paper a HQET sum rule determination of the five $\Delta B = 2$ Bag parameters describing B_s-mixing in the SM and beyond. For that we had to determine m_s and m_s^2 corrections to the three-point correlator at the 3-loop level. In particular we obtain the most precise values for the ratios of Bag parameters in the B_s and B_d system.

JHEP05(2019)034

Combing this result with the most recent lattice results for f_{B_s}/f_{B_d} [18, 42, 44] we obtain the world's most precise value for the ratio

$$\xi \equiv \frac{f_{B_s}}{f_B}\sqrt{\overline{B}_{Q_1}^{s/d}} = 1.2014^{+0.0065}_{-0.0072}\,, \tag{4.1}$$

which represents a reduction of the uncertainty by more than a factor of two compared to the latest lattice results [12, 17]. Our results enable a rich phenomenology: we get updated SM predictions for the mixing observables ΔM_s and $\Delta\Gamma_s$, which are in agreement with the experimental values. In particular we do not confirm the large values for ΔM_s obtained with the non-perturbative values from FNAL/MILC [12], which led to severe bounds on BSM models. If V_{tb} and ΔM_q are used as inputs, we can precisely determine the CKM elements $|V_{td}|$ and $|V_{ts}|$ and we obtain the world's most precise determination of the ratio $|V_{td}/V_{ts}|$. Using all CKM elements as inputs we get constraints on the values of the top quark $\overline{\text{MS}}$ mass which are compatible with direct collider determinations. Finally our results lead also to precise SM predictions for the branching ratios of the rare decays $B_q \to ll$.

In future a still higher precision of our HEQT sum rule results can be obtained by the calculation of the HQET-QCD matching at NNLO (first steps in that direction have been performed in [16]). Another line of improvement could be the determination of $1/m_b$-corrections to the HQET limit. The computation of m_s corrections to the Bag parameters of $\Delta F = 0$ four-quark operators would enable an update of the predictions for the lifetime ratios $\tau(B_s)/\tau(B^0)$ [15] and $\tau(D_s^+)/\tau(D^0)$ [73]. Finally a cross-check of our HQET sum results for mixing and lifetimes with modern lattice techniques would be very desirable.

Acknowledgments

We thank Sébastien Descotes-Genon for providing us with the result (3.17), Oliver Witzel for interesting discussions and Andrzej Buras, Aleksei Rusov and Tobias Tsang for comments on the manuscript. This work was supported by the STFC through the IPPP grant and a Postgraduate Studentship.

JHEP05(2019)034

A Inputs and detailed overview of uncertainties

Parameter	Value	Source
$\overline{m}_b(\overline{m}_b)$	$(4.203^{+0.016}_{-0.034})$ GeV	[74, 75]
$m_b^{\rm PS}(2\text{ GeV})$	$(4.532^{+0.013}_{-0.039})$ GeV	[74, 75]
$\overline{m}_c(\overline{m}_c)$	(1.279 ± 0.013) GeV	[76]
$m_t^{\rm pole}$	(173.0 ± 0.4) GeV	[37]
$\alpha_s(M_Z)$	0.1181 ± 0.0011	[37]
V_{us}	$0.224745^{+0.000254}_{-0.000059}$	[49]
V_{ub}	$0.003746^{+0.000090}_{-0.000062}$	[49]
V_{cb}	$0.04240^{+0.00030}_{-0.00115}$	[49]
γ	$(65.81^{+0.99}_{-1.66})^\circ$	[49]
f_B	(190.0 ± 1.3) MeV	[18]
f_{B_s}	(230.3 ± 1.3) MeV	[18]
f_{B_s}/f_B	1.209 ± 0.005	[18]
$\tau(B_s^{0,\rm H})$	(1.615 ± 0.009) ps^{-1}	[37]
$\tau(B_d^0)$	(1.520 ± 0.004) ps^{-1}	[37]

Table 1. Input values for parameters.

	$\overline{\Lambda}$	intrinsic SR	condensates	μ_ρ	m_s	$1/m_b$	μ_m	a_i
$\overline{B}^s_{Q_1}$	$^{+0.002}_{-0.003}$	±0.018	±0.004	$^{+0.013}_{-0.027}$	$^{+0.003}_{-0.002}$	±0.010	$^{+0.044}_{-0.038}$	$^{+0.007}_{-0.008}$
$\overline{B}^s_{Q_2}$	$^{+0.012}_{-0.014}$	±0.020	±0.004	$^{+0.010}_{-0.015}$	$^{+0.004}_{-0.004}$	±0.010	$^{+0.072}_{-0.063}$	$^{+0.015}_{-0.015}$
$\overline{B}^s_{Q_3}$	$^{+0.047}_{-0.055}$	±0.107	±0.023	$^{+0.026}_{-0.001}$	$^{+0.024}_{-0.026}$	±0.010	$^{+0.091}_{-0.073}$	$^{+0.054}_{-0.053}$
$\overline{B}^s_{Q_4}$	$^{+0.006}_{-0.005}$	±0.021	±0.011	$^{+0.000}_{-0.002}$	$^{+0.003}_{-0.002}$	±0.010	$^{+0.088}_{-0.079}$	$^{+0.006}_{-0.006}$
$\overline{B}^s_{Q_5}$	$^{+0.014}_{-0.012}$	±0.018	±0.009	$^{+0.000}_{-0.007}$	$^{+0.007}_{-0.006}$	±0.010	$^{+0.075}_{-0.067}$	$^{+0.012}_{-0.012}$

Table 2. Individual errors for the Bag parameters in the B_s system.

	$\overline{\Lambda}$	intrinsic SR	condensates	μ_ρ	m_s	$1/m_b$	μ_m	a_i
$\overline{B}^{s/d}_{Q_1}$	$^{+0.001}_{-0.002}$	±0.005	±0.002	$^{+0.002}_{-0.006}$	$^{+0.003}_{-0.002}$	±0.002	$^{+0.000}_{-0.000}$	$^{+0.000}_{-0.000}$
$\overline{B}^{s/d}_{Q_2}$	$^{+0.004}_{-0.003}$	±0.005	±0.002	$^{+0.005}_{-0.002}$	$^{+0.005}_{-0.004}$	±0.002	$^{+0.000}_{-0.000}$	$^{+0.000}_{-0.000}$
$\overline{B}^{s/d}_{Q_3}$	$^{+0.036}_{-0.023}$	±0.025	±0.010	$^{+0.042}_{-0.019}$	$^{+0.029}_{-0.031}$	±0.002	$^{+0.004}_{-0.005}$	$^{+0.005}_{-0.005}$
$\overline{B}^{s/d}_{Q_4}$	$^{+0.001}_{-0.002}$	±0.005	±0.002	$^{+0.002}_{-0.005}$	$^{+0.003}_{-0.002}$	±0.002	$^{+0.000}_{-0.000}$	$^{+0.000}_{-0.000}$
$\overline{B}^{s/d}_{Q_5}$	$^{+0.003}_{-0.004}$	±0.005	±0.002	$^{+0.004}_{-0.010}$	$^{+0.006}_{-0.006}$	±0.002	$^{+0.000}_{-0.000}$	$^{+0.000}_{-0.000}$

Table 3. Individual errors for the ratio of Bag parameters in the B_s and B_d system.

JHEP05(2019)034

	$\Delta M_s^{\rm SM}$ [ps^{-1}]	$\Delta\Gamma_s^{\rm PS}$ [ps^{-1}]	$\Delta M_d^{\rm SM}$ [ps^{-1}]	$\Delta\Gamma_d^{\rm SM}$ [10^{-3}ps^{-1}]
$\overline{B}^q_{Q_1}$	± 1.1	± 0.005	± 0.031	$^{+0.16}_{-0.15}$
$\overline{B}^q_{Q_3}$	± 0.0	$^{+0.006}_{-0.005}$	± 0.000	$^{+0.17}_{-0.16}$
$\overline{B}^q_{R_0}$	± 0.0	± 0.004	± 0.000	± 0.10
$\overline{B}^q_{R_1}$	± 0.0	± 0.000	± 0.000	± 0.01
$\overline{B}^q_{R'_1}$	± 0.0	± 0.000	± 0.000	± 0.01
$\overline{B}^q_{R_2}$	± 0.0	± 0.018	± 0.000	± 0.53
$\overline{B}^q_{R_3}$	± 0.0	± 0.000	± 0.000	± 0.00
$\overline{B}^q_{R'_3}$	± 0.0	± 0.000	± 0.000	± 0.01
f_{B_q}	± 0.2	± 0.001	$^{+0.008}_{-0.007}$	± 0.04
μ_1	± 0.0	$^{+0.008}_{-0.021}$	± 0.000	$^{+0.24}_{-0.60}$
μ_2	± 0.1	$^{+0.000}_{-0.003}$	$^{+0.004}_{-0.002}$	$^{+0.00}_{-0.08}$
m_b	± 0.0	$^{+0.000}_{-0.001}$	± 0.000	$^{+0.01}_{-0.04}$
m_c	± 0.0	± 0.001	± 0.000	± 0.02
α_s	± 0.0	± 0.000	± 0.001	± 0.01
CKM	$^{+0.3}_{-1.0}$	$^{+0.001}_{-0.005}$	$^{+0.011}_{-0.032}$	$^{+0.06}_{-0.15}$

Table 4. Individual errors for the B_s and B_d mixing observables.

References

[1] M. Artuso, G. Borissov and A. Lenz, *CP violation in the B_s^0 system*, *Rev. Mod. Phys.* **88** (2016) 045002 [arXiv:1511.09466] [INSPIRE].

[2] HFLAV collaboration, *Averages of b-hadron, c-hadron and τ-lepton properties as of summer 2016*, *Eur. Phys. J.* **C 77** (2017) 895 [arXiv:1612.07233] [INSPIRE].

[3] CDF collaboration, *Observation of B_s^0-$\bar{B}_s^0$ oscillations*, *Phys. Rev. Lett.* **97** (2006) 242003 [hep-ex/0609040] [INSPIRE].

[4] LHCb collaboration, *Measurement of the $B_s^0 - \bar{B}_s^0$ oscillation frequency Δm_s in $B_s^0 \to D_s^-(3)\pi$ decays*, *Phys. Lett.* **B 709** (2012) 177 [arXiv:1112.4311] [INSPIRE].

[5] LHCb collaboration, *Precision measurement of the B_s^0-$\bar{B}_s^0$ oscillation frequency with the decay $B_s^0 \to D_s^-\pi^+$*, *New J. Phys.* **15** (2013) 053021 [arXiv:1304.4741] [INSPIRE].

[6] LHCb collaboration, *Observation of B_s^0-$\bar{B}_s^0$ mixing and measurement of mixing frequencies using semileptonic B decays*, *Eur. Phys. J.* **C 73** (2013) 2655 [arXiv:1308.1302] [INSPIRE].

[7] LHCb collaboration, *Precision measurement of CP violation in $B_s^0 \to J/\psi K^+K^-$ decays*, *Phys. Rev. Lett.* **114** (2015) 041801 [arXiv:1411.3104] [INSPIRE].

[8] T. Inami and C.S. Lim, *Effects of superheavy quarks and leptons in low-energy weak processes $k_L \to \mu\bar{\mu}$, $K^+ \to \pi^+\nu\bar{\nu}$ and $K^0 \leftrightarrow \bar{K}^0$*, *Prog. Theor. Phys.* **65** (1981) 297 [*Erratum ibid.* **65** (1981) 1772] [INSPIRE].

JHEP05(2019)034

[9] A.J. Buras, M. Jamin and P.H. Weisz, *Leading and Next-to-leading QCD corrections to ϵ parameter and B^0-$\bar{B}^0$ mixing in the presence of a heavy top quark*, *Nucl. Phys.* **B 347** (1990) 491 [INSPIRE].

[10] E. Dalgic et al., *B_s^0-$\bar{B}_s^0$ mixing parameters from unquenched lattice QCD*, *Phys. Rev.* **D 76** (2007) 011501 [hep-lat/0610104] [INSPIRE].

[11] ETM collaboration, *B-physics from $N_f = 2$ tmQCD: the Standard Model and beyond*, *JHEP* **03** (2014) 016 [arXiv:1308.1851] [INSPIRE].

[12] Fermilab Lattice, MILC collaboration, *$B^0_{(s)}$-mixing matrix elements from lattice QCD for the Standard Model and beyond*, *Phys. Rev.* **D 93** (2016) 113016 [arXiv:1602.03560] [INSPIRE].

[13] A.G. Grozin, R. Klein, T. Mannel and A.A. Pivovarov, *B^0-$\bar{B}^0$ mixing at next-to-leading order*, *Phys. Rev.* **D 94** (2016) 034024 [arXiv:1606.06054] [INSPIRE].

[14] A.G. Grozin, T. Mannel and A.A. Pivovarov, *Towards a next-to-next-to-leading order analysis of matching in B^0-$\bar{B}^0$ mixing*, *Phys. Rev.* **D 96** (2017) 074032 [arXiv:1706.05910] [INSPIRE].

[15] M. Kirk, A. Lenz and T. Rauh, *Dimension-six matrix elements for meson mixing and lifetimes from sum rules*, *JHEP* **12** (2017) 068 [arXiv:1711.02100] [INSPIRE].

[16] A.G. Grozin, T. Mannel and A.A. Pivovarov, *B^0-$\bar{B}^0$ mixing: Matching to HQET at NNLO*, *Phys. Rev.* **D 98** (2018) 054020 [arXiv:1806.00253] [INSPIRE].

[17] RBC/UKQCD collaboration, *SU(3)-breaking ratios for $D_{(s)}$ and $B_{(s)}$ mesons*, arXiv:1812.08791 [INSPIRE].

[18] Flavour Lattice Averaging Group collaboration, *FLAG review 2019*, arXiv:1902.08191 [INSPIRE].

[19] L. Di Luzio, M. Kirk and A. Lenz, *Updated B_s-mixing constraints on new physics models for $b \to s\ell^+\ell^-$ anomalies*, *Phys. Rev.* **D 97** (2018) 095035 [arXiv:1712.06572] [INSPIRE].

[20] F. Gabbiani, E. Gabrielli, A. Masiero and L. Silvestrini, *A complete analysis of FCNC and CP constraints in general SUSY extensions of the standard model*, *Nucl. Phys.* **B 477** (1996) 321 [hep-ph/9604387] [INSPIRE].

[21] E. Eichten and B.R. Hill, *An Effective field theory for the calculation of matrix elements involving heavy quarks*, *Phys. Lett.* **B 234** (1990) 511 [INSPIRE].

[22] D.J. Broadhurst and A.G. Grozin, *Operator product expansion in static quark effective field theory: large perturbative correction*, *Phys. Lett.* **B 274** (1992) 421 [hep-ph/9908363] [INSPIRE].

[23] E. Bagan, P. Ball, V.M. Braun and H.G. Dosch, *QCD sum rules in the effective heavy quark theory*, *Phys. Lett.* **B 278** (1992) 457 [INSPIRE].

[24] M. Neubert, *Heavy meson form-factors from QCD sum rules*, *Phys. Rev.* **D 45** (1992) 2451 [INSPIRE].

[25] S.C. Generalis, *Improved two loop quark mass corrections*, *J. Phys.* **G 15** (1989) L225 [INSPIRE].

[26] M. Beneke and V.A. Smirnov, *Asymptotic expansion of Feynman integrals near threshold*, *Nucl. Phys.* **B 522** (1998) 321 [hep-ph/9711391] [INSPIRE].

JHEP05(2019)034

[27] B. Jantzen, *Foundation and generalization of the expansion by regions*, *JHEP* **12** (2011) 076 [arXiv:1111.2589] [INSPIRE].

[28] K.G. Chetyrkin, A.L. Kataev, A.B. Krasulin and A.A. Pivovarov, *Calculation of the K^0-$\bar{K}^0$ mixing parameter via the QCD sum rules at finite energies*, *Phys. Lett.* **B 174** (1986) 104 [hep-ph/0103230] [INSPIRE].

[29] J.G. Korner, A.I. Onishchenko, A.A. Petrov and A.A. Pivovarov, *B^0-$\bar{B}^0$ mixing beyond factorization*, *Phys. Rev. Lett.* **91** (2003) 192002 [hep-ph/0306032] [INSPIRE].

[30] P. Nogueira, *Automatic Feynman graph generation*, *J. Comput. Phys.* **105** (1993) 279 [INSPIRE].

[31] M. Jamin and M.E. Lautenbacher, *TRACER: Version 1.1: a Mathematica package for gamma algebra in arbitrary dimensions*, *Comput. Phys. Commun.* **74** (1993) 265 [INSPIRE].

[32] A.V. Smirnov, *FIRE5: a C++ implementation of Feynman Integral REduction*, *Comput. Phys. Commun.* **189** (2015) 182 [arXiv:1408.2372] [INSPIRE].

[33] K.G. Chetyrkin and F.V. Tkachov, *Integration by parts: the algorithm to calculate β-functions in 4 loops*, *Nucl. Phys.* **B 192** (1981) 159 [INSPIRE].

[34] S. Laporta, *High precision calculation of multiloop Feynman integrals by difference equations*, *Int. J. Mod. Phys.* **A 15** (2000) 5087 [hep-ph/0102033] [INSPIRE].

[35] A.G. Grozin and R.N. Lee, *Three-loop HQET vertex diagrams for B^0-$\bar{B}^0$ mixing*, *JHEP* **02** (2009) 047 [arXiv:0812.4522] [INSPIRE].

[36] T. Huber and D. Maître, *HypExp 2, expanding hypergeometric functions about half-integer parameters*, *Comput. Phys. Commun.* **178** (2008) 755 [arXiv:0708.2443] [INSPIRE].

[37] Particle Data Group collaboration, *Review of particle physics*, *Phys. Rev.* **D 98** (2018) 030001 [INSPIRE].

[38] T. Mannel, B.D. Pecjak and A.A. Pivovarov, *Sum rule estimate of the subleading non-perturbative contributions to B_s-$\bar{B}_s$ mixing*, *Eur. Phys. J.* **C 71** (2011) 1607 [hep-ph/0703244] [INSPIRE].

[39] T. Mannel, B.D. Pecjak and A.A. Pivovarov, *Sum rule estimate of the subleading non-perturbative contributions to B_s-$\bar{B}_s$ mixing*, *Eur. Phys. J.* **C 71** (2011) 1607 [hep-ph/0703244] [INSPIRE].

[40] C. McNeile et al., *Direct determination of the strange and light quark condensates from full lattice QCD*, *Phys. Rev.* **D 87** (2013) 034503 [arXiv:1211.6577] [INSPIRE].

[41] HPQCD collaboration, *Determination of the quark condensate from heavy-light current-current correlators in full lattice QCD*, arXiv:1811.04305 [INSPIRE].

[42] A. Bazavov et al., *B- and D-meson leptonic decay constants from four-flavor lattice QCD*, *Phys. Rev.* **D 98** (2018) 074512 [arXiv:1712.09262] [INSPIRE].

[43] P. Boyle et al., *BSM kaon mixing at the physical point*, *EPJ Web Conf.* **175** (2018) 13010 [arXiv:1710.09176] [INSPIRE].

[44] C. Hughes, C.T.H. Davies and C.J. Monahan, *New methods for B meson decay constants and form factors from lattice NRQCD*, *Phys. Rev.* **D 97** (2018) 054509 [arXiv:1711.09981] [INSPIRE].

[45] HPQCD collaboration, *Neutral B meson mixing in unquenched lattice QCD*, *Phys. Rev.* **D 80** (2009) 014503 [arXiv:0902.1815] [INSPIRE].

JHEP05(2019)034

[46] M. Beneke, *A quark mass definition adequate for threshold problems*, *Phys. Lett.* **B 434** (1998) 115 [hep-ph/9804241] [INSPIRE].

[47] A.H. Hoang, Z. Ligeti and A.V. Manohar, *B decay and the Υ mass*, *Phys. Rev. Lett.* **82** (1999) 277 [hep-ph/9809423] [INSPIRE].

[48] I.I.Y. Bigi, M.A. Shifman, N. Uraltsev and A.I. Vainshtein, *High power n of m_b in beauty widths and $N = 5 \to \infty$ limit*, *Phys. Rev.* **D 56** (1997) 4017 [hep-ph/9704245] [INSPIRE].

[49] CKMFITTER GROUP collaboration, *CP violation and the CKM matrix: Assessing the impact of the asymmetric B factories*, *Eur. Phys. J.* **C 41** (2005) 1 [hep-ph/0406184] [INSPIRE].

[50] E. Govorkova, *Mixing and time-dependent CP violation in beauty at LHCb*, talk given at the 54th *Rencontres de Moriond on Electroweak Interactions and Unified Theories (Moriond EW 2019)*, March 16–23, La Thuile, Italy (2019).

[51] O. Igonkina, *B-physics results in ATLAS in Run2*, talk given at the 54th *Rencontres de Moriond on Electroweak Interactions and Unified Theories (Moriond EW 2019)*, March 16–23, La Thuile, Italy (2019).

[52] M. Beneke et al., *Next-to-leading order QCD corrections to the lifetime difference of B_s mesons*, *Phys. Lett.* **B 459** (1999) 631 [hep-ph/9808385] [INSPIRE].

[53] M. Beneke, G. Buchalla, A. Lenz and U. Nierste, *CP asymmetry in flavor specific B decays beyond leading logarithms*, *Phys. Lett.* **B 576** (2003) 173 [hep-ph/0307344] [INSPIRE].

[54] M. Ciuchini et al., *Lifetime differences and CP-violation parameters of neutral B mesons at the next-to-leading order in QCD*, *JHEP* **08** (2003) 031 [hep-ph/0308029] [INSPIRE].

[55] A. Lenz and U. Nierste, *Theoretical update of B_s-$\bar{B}_s$ mixing*, *JHEP* **06** (2007) 072 [hep-ph/0612167] [INSPIRE].

[56] M. Beneke, G. Buchalla and I. Dunietz, *Width difference in the B_s-$\bar{B}_s$ system*, *Phys. Rev.* **D 54** (1996) 4419 [*Erratum ibid.* **D 83** (2011) 119902] [hep-ph/9605259] [INSPIRE].

[57] A.S. Dighe, T. Hurth, C.S. Kim and T. Yoshikawa, *Measurement of the lifetime difference of B_d mesons: possible and worthwhile?*, *Nucl. Phys.* **B 624** (2002) 377 [hep-ph/0109088] [INSPIRE].

[58] H.M. Asatrian, A. Hovhannisyan, U. Nierste and A. Yeghiazaryan, *Towards next-to-next-to-leading-log accuracy for the width difference in the B_s-$\bar{B}_s$ system: fermionic contributions to order $(m_c/m_b)^0$ and $(m_c/m_b)^1$*, *JHEP* **10** (2017) 191 [arXiv:1709.02160] [INSPIRE].

[59] UTFIT collaboration, *The Unitarity Triangle Fit in the standard model and hadronic parameters from lattice QCD: a reappraisal after the measurements of Δm_s and $BR(B \to \tau\nu_\tau)$*, *JHEP* **10** (2006) 081 [hep-ph/0606167] [INSPIRE].

[60] M. Blanke and A.J. Buras, *Emerging ΔM_d-anomaly from tree-level determinations of $|V_{cb}|$ and the angle γ*, *Eur. Phys. J.* **C 79** (2019) 159 [arXiv:1812.06963] [INSPIRE].

[61] M. Blanke and A.J. Buras, *Universal Unitarity Triangle 2016 and the tension between $\Delta M_{s,d}$ and ε_K in CMFV models*, *Eur. Phys. J.* **C 76** (2016) 197 [arXiv:1602.04020] [INSPIRE].

[62] A.V. Bednyakov, B.A. Kniehl, A.F. Pikelner and O.L. Veretin, *Stability of the electroweak vacuum: gauge independence and advanced precision*, *Phys. Rev. Lett.* **115** (2015) 201802 [arXiv:1507.08833] [INSPIRE].

JHEP05(2019)034

[63] A.H. Hoang, S. Plätzer and D. Samitz, *On the cutoff dependence of the quark mass parameter in angular ordered parton showers*, *JHEP* **10** (2018) 200 [arXiv:1807.06617] [INSPIRE].

[64] M. Beneke et al., *Next-to-next-to-next-to-leading order QCD prediction for the top antitop S-wave pair production cross section near threshold in e^+e^- annihilation*, *Phys. Rev. Lett.* **115** (2015) 192001 [arXiv:1506.06864] [INSPIRE].

[65] M. Beneke, A. Maier, T. Rauh and P. Ruiz-Femenia, *Non-resonant and electroweak NNLO correction to the e^+e^- top anti-top threshold*, *JHEP* **02** (2018) 125 [arXiv:1711.10429] [INSPIRE].

[66] F. Simon, *Impact of theory uncertainties on the precision of the top quark mass in a threshold scan at future e^+e^- colliders*, PoS(ICHEP2016)872 [arXiv:1611.03399] [INSPIRE].

[67] C. Bobeth et al., *$B_{s,d} \to l^+l^-$ in the standard model with reduced theoretical uncertainty*, *Phys. Rev. Lett.* **112** (2014) 101801 [arXiv:1311.0903] [INSPIRE].

[68] A.J. Buras, *Relations between $\Delta M_{s,d}$ and $B_{s,d} \to \mu\bar{\mu}$ in models with minimal flavor violation*, *Phys. Lett.* **B 566** (2003) 115 [hep-ph/0303060] [INSPIRE].

[69] M. Beneke, C. Bobeth and R. Szafron, *Enhanced electromagnetic correction to the rare B-meson decay $B_{s,d} \to \mu^+\mu^-$*, *Phys. Rev. Lett.* **120** (2018) 011801 [arXiv:1708.09152] [INSPIRE].

[70] CMS collaboration, *Measurement of the $B_s^0 \to \mu^+\mu^-$ branching fraction and search for $B^0 \to \mu^+\mu^-$ with the CMS Experiment*, *Phys. Rev. Lett.* **111** (2013) 101804 [arXiv:1307.5025] [INSPIRE].

[71] LHCb collaboration, *Measurement of the $B_s^0 \to \mu^+\mu^-$ branching fraction and effective lifetime and search for $B^0 \to \mu^+\mu^-$ decays*, *Phys. Rev. Lett.* **118** (2017) 191801 [arXiv:1703.05747] [INSPIRE].

[72] ATLAS collaboration, *Study of the rare decays of B_s^0 and B^0 mesons into muon pairs using data collected during 2015 and 2016 with the ATLAS detector*, *JHEP* **04** (2019) 098 [arXiv:1812.03017] [INSPIRE].

[73] A. Lenz and T. Rauh, *D-meson lifetimes within the heavy quark expansion*, *Phys. Rev.* **D 88** (2013) 034004 [arXiv:1305.3588] [INSPIRE].

[74] M. Beneke, A. Maier, J. Piclum and T. Rauh, *The bottom-quark mass from non-relativistic sum rules at NNNLO*, *Nucl. Phys.* **B 891** (2015) 42 [arXiv:1411.3132] [INSPIRE].

[75] M. Beneke, A. Maier, J. Piclum and T. Rauh, *NNNLO determination of the bottom-quark mass from non-relativistic sum rules*, PoS(RADCOR2015)035 [arXiv:1601.02949] [INSPIRE].

[76] K.G. Chetyrkin et al., *Charm and bottom quark masses: an update*, *Phys. Rev.* **D 80** (2009) 074010 [arXiv:0907.2110] [INSPIRE].

JHEP05(2019)034